RESEARCH ARTICLE

Synthetic auxotrophy reveals metabolic regulation of plasma cell generation, affinity maturation, and cytokine receptor signaling

Sung Hoon Cho[1*†‡], Shawna K Brookens[1,2†], Ariel L Raybuck[1†], Kaylor Meyer[1†], Yeeun Paik[1†], Jennie Hamilton[1], Jingxin Li[1], Karel Kalecky[3], Chloe Park[1], Juyeon Lim[1], Sakeenah L Hicks[4], John Karijolich[1], Teodoro H Bottiglieri[3], Jeffrey C Rathmell[1,5,6], Denis Mogilenko[5,6,7], Christopher D Scharer[4], Mark R Boothby[1,2,5,6,7*]

[1]Department of Pathology, Microbiology and Immunology, Molecular Pathogenesis Division, Vanderbilt University Medical Center, Nashville, United States; [2]Cancer Biology Program, Vanderbilt University, Nashville, United States; [3]Center of Metabolomics, Institute of Metabolic Disease, Baylor Scott and White Research Institute, Dallas, United States; [4]Department of Microbiology and Immunology, Emory University School of Medicine, Atlanta, United States; [5]Vanderbilt Center for Immunobiology, Vanderbilt University Medical Center, Nashville, United States; [6]Vanderbilt Center for Infection, Inflammation, Immunology (VI4), Vanderbilt University Medical Center, Nashville, United States; [7]Department of Medicine, Rheumatology and Immunology Division, Vanderbilt University Medical Center, Nashville, United States

***For correspondence:** sung.hoon.cho@emory.edu (SHC); mark.boothby@vumc.org (MRB)

[†]These authors contributed equally to this work.

Present address: [‡]Department of Medicine, Division of Rheumatology, Emory University School of Medicine, Atlanta, United States

Competing interest: See page 27

Funding: See page 27

Preprint posted
09 May 2025
Sent for Review
26 May 2025
Reviewed preprint v1
18 August 2025
Reviewed preprint v2
18 August 2026
Version of Record
29 October 2026

Reviewing Editor: Tomohiro Kurosaki, The University of Osaka, Japan

© Copyright Cho, Brookens, Raybuck *et al*. This article is distributed under the terms of the Creative Commons Attribution License, which permits unrestricted use and redistribution provided that the original author and source are credited.

eLife Assessment

The authors addressed a significant biological question, namely the role of glutamine metabolism in humoral responses, and they obtained **solid** conclusions. The strength of this study is that the authors used state-of-the-art transgenic mouse models together with in vitro analysis, thereby providing **important** insights into the question posed. The manuscript has been further substantiated by adding more appropriate experimental controls and describing more in-depth functionality/physiological relevance.

Abstract The proliferation and development of activated B lymphocytes into antibody (Ab)-secreting plasma cells are critical determinants of humoral immunity and sustain certain autoimmune diseases. Specific pathways and substrate supplies in intermediary metabolism influence lymphocyte differentiation and function. We now show that although stringent restriction of glutamine supply decreases B cell proliferation and differentiation into plasma cells, glutaminolysis – a major metabolic use of this amino acid – was only conditionally crucial in B cells and the Ab responses derived from them. *Gls*, the gene encoding the main glutaminase of lymphocytes, promoted anti-NP Ab responses at the primary and recall phases if either glucose uptake into mouse B cells or pyruvate into their mitochondria was also impaired. Otherwise, it was dispensable. This synthetic auxotrophy, that is, the conditional requirement of glutaminase for processes in addition to survival, involved supporting progressive expansion of mitochondrial respiration followed by plasma cell differentiation. Surprisingly, impairment of glutaminase and the mitochondrial pyruvate channel decreased

IL-21 stimulation of STAT3 phosphorylation as well as interferon stimulation of STAT1 activation. Together, our findings establish a powerful collaboration of metabolic pathways in programming increased respiration and the development of Ab-secreting cells, but also reveal modulation of cytokine receptor signaling by metabolism.

Introduction

Circulating antibodies (Ab) are crucial mediators of protection against potentially pathogenic microbes, but Ab also can cause tissue damage or cellular dysfunction (***Geyer et al., 2021***; ***McGettigan and Debes, 2021***; ***Olsen and Karp, 2014***; ***Suurmond and Diamond, 2015***; ***Tsokos et al., 2016***). In both adaptive and pathological settings, Ab functions depend on their heavy chain class, affinity, and concentration (reviewed in ***Rajewsky, 1996***; ***Lu et al., 2018***; ***Alemán and Rosales, 2023***). Increased affinity after initial and repeated immunizations can be selected in several ways, one of which involves processes that occur in the microanatomy of germinal centers (also known as secondary follicles; reviewed in ***Boothby et al., 2019***; ***Elsner and Shlomchik, 2020***; ***Victora and Nussenzweig, 2022***). Progeny cells that survive a gauntlet of programmed death in selecting for continued clonal proliferation ultimately can generate either memory B cells (MBCs) or an end-stage descendant of the B lineage, the plasma cell (PC) (***Victora and Nussenzweig, 2022***; ***Good-Jacobson and Shlomchik, 2010***; ***Adachi et al., 2015***; ***Leach et al., 2019***; ***Inoue and Kurosaki, 2024***). The magnitude of PC output (the numbers generated after B cell activation) and their rates of immunoglobulin secretion (***Inoue and Kurosaki, 2024***; ***Ise and Kurosaki, 2019***; ***Eyer et al., 2017***; ***Eyer et al., 2020***) determine the net output and steady-state concentrations of Ab. Accordingly, understanding mechanisms that regulate the qualities or quantities of Ab, and that reduce or enhance the efficiency of generating PC, are important goals.

To elicit protective Ab, immune exposures such as vaccination activate B cell proliferation, and some progeny of such activated B cells develop into Ab-secreting PC (***Shapiro-Shelef and Calame, 2005***; ***Robinson et al., 2020***; ***Bhattacharya, 2022***). Specificity is fostered by a reliance on signal initiation through the BCR, the clonal Ag receptor on mature B lymphocytes (***Paus et al., 2006***; ***Phan et al., 2006***; ***Benson et al., 2007***). The capacity to be activated, survival efficiency, rates of proliferation, and propensity to yield GC B cells or PC depend on an array of other signal-initiating receptors, among them CD19, co-stimulators such as CD40 (reviewed in ***Elgueta et al., 2009***; ***Rathmell et al., 1996***), the death receptor Fas (***Rathmell et al., 1996***), pattern recognition receptors in the TLR family (***Eckl-Dorna and Batista, 2009***; reviewed in ***Celhar et al., 2012***; ***Fillatreau et al., 2021***), and cytokine receptors (***King and Mohrs, 2009***; ***Pignarre et al., 2021***; ***Duan et al., 2021***; ***Ozaki et al., 2002***; ***Ettinger et al., 2005***). One consequence of activation is that B lymphoblasts dramatically increase expression of an array of nutrient transporters that include those for amino acids and for glucose (***Caro-Maldonado et al., 2014***; ***Cho et al., 2016***; reviewed in ***Boothby et al., 2022***). Beyond this general picture, however, the effects or outputs of receptors likely are scalar and conditional, that is dependent on other signals. For instance, antigen with a high affinity and high valency of the BCR epitope signals differently from a monovalent, lower-affinity antigen (***Kurosaki, 1999***; ***Marshall et al., 2000***; ***Puffer et al., 2007***; ***Mukherjee et al., 2013***; ***Pone et al., 2022***; ***Kato et al., 2020***, reviewed in ***Kwak et al., 2019***), and may influence generation of PC. Moreover, increased expression of TLR7 or type 1 interferon (IFN) receptor stimulation each reduces the capacity of B cells to maintain self-tolerance (***Banchereau and Pascual, 2006***; ***Green and Marshak-Rothstein, 2011***; ***Hamilton et al., 2017***; ***Domeier et al., 2018***), presumably involving changes in the quantitative balance among signal transducers and transcription factors. At a later stage, the IL-21 receptor is crucial for PC differentiation (***Ozaki et al., 2002***). Moreover, IL-21 has recently been reported to promote affinity maturation of GC-derived PC (***MacLean et al., 2025***). Little is known about the relationships between signal strength and metabolism. In vitro experiments showed that hypoxia or genetically mediated stabilization of hypoxia-inducible transcription factors (HIFs) blunted activation-induced increases in amino acid uptake and transporter gene expression as well as GC and Ab responses (***Cho et al., 2016***; ***Li et al., 2021***). However, it remains unclear if metabolism can modulate signaling.

Nonetheless, a substantial and increasing body of evidence indicates that nutrient supply, uptake, and intermediary metabolism influence the properties of adaptive immunity, in part by their effects on differentiation and function of cells that mediate host responses (reviewed in ***Pignarre et al., 2021***;

Edinger, 2007; *Johnson et al., 2016*; *Ripperger and Bhattacharya, 2021*). The bulk of evidence is from analyses of the differentiation and functions of T cells, macrophages, and dendritic cells and documents condition and cell type specificity of findings. Nonetheless, several analyses point to important effects on B cells as well. In addition to a function during B cell development, expression of the glucose transporter (GLUT)1 on mature B cells supported the initial GC size, the Ag-specific Ab responses derived from B cells, and affinity maturation (*Caro-Maldonado et al., 2014*; *Brookens et al., 2024*; *Bierling et al., 2024*).

Among nutrients, only the distribution and sufficiency of oxygen are readily measured, but such analyses consistently reveal evidence of functional hypoxia in follicles, most accentuated in GC (*Cho et al., 2016*; *Li et al., 2021*; *Jellusova et al., 2017*; *Nakagawa et al., 2024*). Consistent with and potentially as a result of the hypoxia, GC B cells can exhibit higher rates of glucose uptake with several-fold increased glucose oxidation as well as utilization in the pentose phosphate pathway (*Cho et al., 2016*; *Brookens et al., 2024*; *Bierling et al., 2024*; *Jellusova et al., 2017*). Moreover, the ability to feed intermediates into one-carbon metabolism via increased expression of the enzyme phosphoglycerate dehydrogenase was reported to be crucial for germinal center size and normal degrees of high-affinity antibody production (*D'Avola et al., 2022*). Cell-type- and stage-specific inactivation of *Slc2a1*, the gene that encodes GLUT1, indicates that the increased glucose uptake is crucial for both GC homeostasis and the capacity of B cells to yield antibody-secreting PC (*Brookens et al., 2024*; *Bierling et al., 2024*). Metabolomic analyses suggested that increases in anaplerotic conversion and usage of amino acids may be evoked in GLUT1-deficient B cells as a potential compensatory mechanism (*Bierling et al., 2024*). In parallel, however, a remarkable degree of metabolic flexibility was suggested by the in vitro finding that although glucose is essential for PC development and Ab production in the absence of other hexoses, mannose, and galactose together could substitute for glucose (*Brookens et al., 2024*). Thus, the reduced influx and availability of glucose reduced Ab responses and affinity maturation, but the decrease in these outputs fell short of what likely could be therapeutically meaningful. Moreover, the importance of feeding the increase in B cell-intrinsic generation of serine with diversion of 3-phosphoglycerate away from generating pyruvate raised the question whether the capacity of mitochondria to use this latter metabolite was important in promoting greater quality and quantity of Ab after immunization.

To explore these issues, we used both immunizations and in vitro analyses that leveraged genetic and pharmacological approaches to test the importance of glutaminolysis – on its own or in combination with a second pathway – in Ab responses. Glutamine concentrations in vitro were found to be crucial for class switching as well as PC and Ab production, and B cell type-restricted inactivation of the *Gls* gene, which encodes the glutaminase expressed in post-natal cells outside the liver, impaired the response to ovalbumin in one immunization model. Surprisingly, however, the anti-NP response in a hapten-carrier model was unaffected. However, a synergistic impact resulted when GLS depletion was combined with targeted loss of function for either GLUT1 (*Slc2a1*) or an essential subunit of a mitochondrial pyruvate import carrier (*Mpc2)* (*Zangari et al., 2020*; *Lam et al., 2016*). Thus, glutaminolysis promoted the anti-NP response only if glucose intake or pyruvate flux was impaired, revealing one limit imposed on the metabolic flexibility of B cells in their mediation of Ab responses. The combined restriction of two pathways that feed mitochondrial metabolism represented what can be termed 'synthetic auxotrophy' rather than synthetic lethality (*Farmer et al., 2005*; *O'Neil et al., 2017*), in that effects on differentiation were observed beyond the impacts on death or proliferation. Gene expression signatures in GC B cells highlighted a requirement for GLS in metabolic reprogramming, that is both amplification of glucose-stimulated proton secretion and a major increase in mitochondrial respiration between the first and second days after B cell activation. Surprisingly, MPC2 and GLS were found to promote not only IL-21-stimulated STAT3 activation but also an IFN response signature in addition to promoting increased respiration. Together, the results reveal that an interplay between two metabolic pathways unexpectedly converged on programming not only IL-21R activation of STAT3, PC differentiation, and high-affinity Ab responses, but also the tyrosyl and serine phosphorylation of STAT1 induced by type 1 and type 2 IFNs. These findings have important implications for diseases, such as systemic lupus erythematosus (SLE), in which B cells and their response to IFN are crucial elements of pathogenesis.

Results

Alpha-ketoglutarate can alter threshold glutamine concentration requirements for B cell responses

B lymphoblasts subjected to persistent stabilization of the HIFs took up amino acids at lower rates in vitro and exhibited decreased mTORC1 activity (***Cho et al., 2016***). mTORC1 promotes Ab class switching by a mechanism beyond effects on the rate of proliferation (***Cho et al., 2016***; ***Raybuck et al., 2018***; ***Jones et al., 2016***), and extracellular glutamine influences class switch recombination in B cells through a mechanism involving the action of mTORC1 on proteins regulating translation (***Chiu et al., 2019***). Other work has provided evidence that plasmablasts developing in the setting of plasmodial infection are glutamine avid (***Vijay et al., 2020***). The admixture of red and white pulp in spleen precludes accurate measurement of amino acid concentrations surrounding B cells in lymphoid follicles. Instead, we adapted a technique used for tumor masses (***Haslene-Hox et al., 2011***; ***Sugiura et al., 2022***) to measure glutamine in the fluid eluted from transected lymph nodes, revealing a strikingly lower concentration than in plasma (***Figure 1a***). This apparent glutamine gradient was not a universal feature of the lymph node, in that neither leucine nor pyruvate differed substantially between plasma and interstitium (***Figure 1a***). To test the dependence of B cells on extracellular glutamine concentration in vitro, and to align with later immunization experiments in which IgG1 is conventionally used as the main readout for isotype-switched Ab responses, we measured both class switching and PC differentiation. Titrations of glutamine in media showed that proliferation, PC differentiation, and the Ab class switch to IgG1 were impaired (***Figure 1b and c***; ***Figure 1—figure supplement 1a–c***). Although not pursued herein, it is intriguing that some aspects of the immune microenvironment appear to support robust switching and PC generation at a glutamine level that would be insufficient in vitro, suggesting that the required concentration is affected by the signals or nutrients in vivo.

Among uses of glutamine after its uptake into cells, glutaminolysis is the first step in generation of α-ketoglutarate (αKG) from the amino acid for usage in the Krebs (TCA) cycle (***Altman et al., 2016***). To screen whether this process might be of functional significance in the molecular regulation of the class-switch or PC differentiation, and to test if the observed effects were purely division-related, we used dye partitioning combined with additions of dimethyl-ketoglutarate (DMK) in vitro. This cell-permeable molecule can bypass glutaminolysis yet supply αKG. The glutamine requirement for switching to IgG1 was almost completely substituted by DMK (***Figure 1d***; ***Figure 1—figure supplement 1b***). Moreover, development of $CD138^+$ cells involved a process beyond just the proliferative effect, in that the $\%CD138^+$ was lowered by glutamine restriction for multiply-divided cells (division peaks 5, 6, and 7; ***Figure 1d***). Interestingly, DMK in the same cultures as used to score switching to IgG1 effected a definite but incomplete reversion of the glutamine requirement in both division rates and in frequencies of switching and differentiation at equal division numbers (***Figure 1d***; ***Figure 1—figure supplement 1b–g***). These findings suggest that although other mechanisms likely also apply, B lymphoblasts need glutaminolysis to supply sufficient αKG to the B lymphoblasts.

Glutaminolysis in B cells promotes an anti-ovalbumin Ab response

Glutamine can be taken up via many distinct transporters, and reduction in one can be compensated by increases in others (***Sugiura et al., 2022***). However, the in vitro data supported testing to what extent immunization-induced Ab responses are affected by glutaminolysis. To bypass potential developmental effects in the B lineage as well as the complex roles of glutamine in T cells and other cell types (***Klysz et al., 2015***; ***Liu et al., 2017***; ***Johnson et al., 2018***), we introgressed a transgene that encodes B lineage-specific expression of a chemically activated recombinase onto a *Gls* f/f background (***Johnson et al., 2018***; ***Khalil et al., 2012***). Inactivation of the *Gls* gene in mature B cells (***Figure 1f***; ***Figure 1—figure supplement 2a, b***) and their descendants, hereafter termed $Gls^{\Delta\Delta}$, by deletion of a segment flanked by loxP sites, could then be initiated at different times after establishment of a normal pre-immune B lineage. Mice (all huCD20-$CreER^{T2}$+/-, and *Gls*+/+ or f/f) in which tamoxifen was administered prior to immunization were sensitized to ovalbumin followed by antigen (Ag) challenge in the airways. Lack of GLS (***Figure 1—figure supplement 2a, b***) led to reduced class-switched GC B cells in lymph nodes draining the lung (***Figure 1g***) as well as the populations of ovalbumin-specific Ab-secreting cells (ASCs) in the lung and bone marrow (***Figure 1h–j***). In line with these data, anti-ovalbumin IgG1 and IgM concentrations in sera of B-specific $Gls^{\Delta\Delta}$ mice were ~0.25 x those of $CreER^{T2}$ controls (***Figure 1k***; ***Figure 1—figure supplement 2c***). We conclude that in these

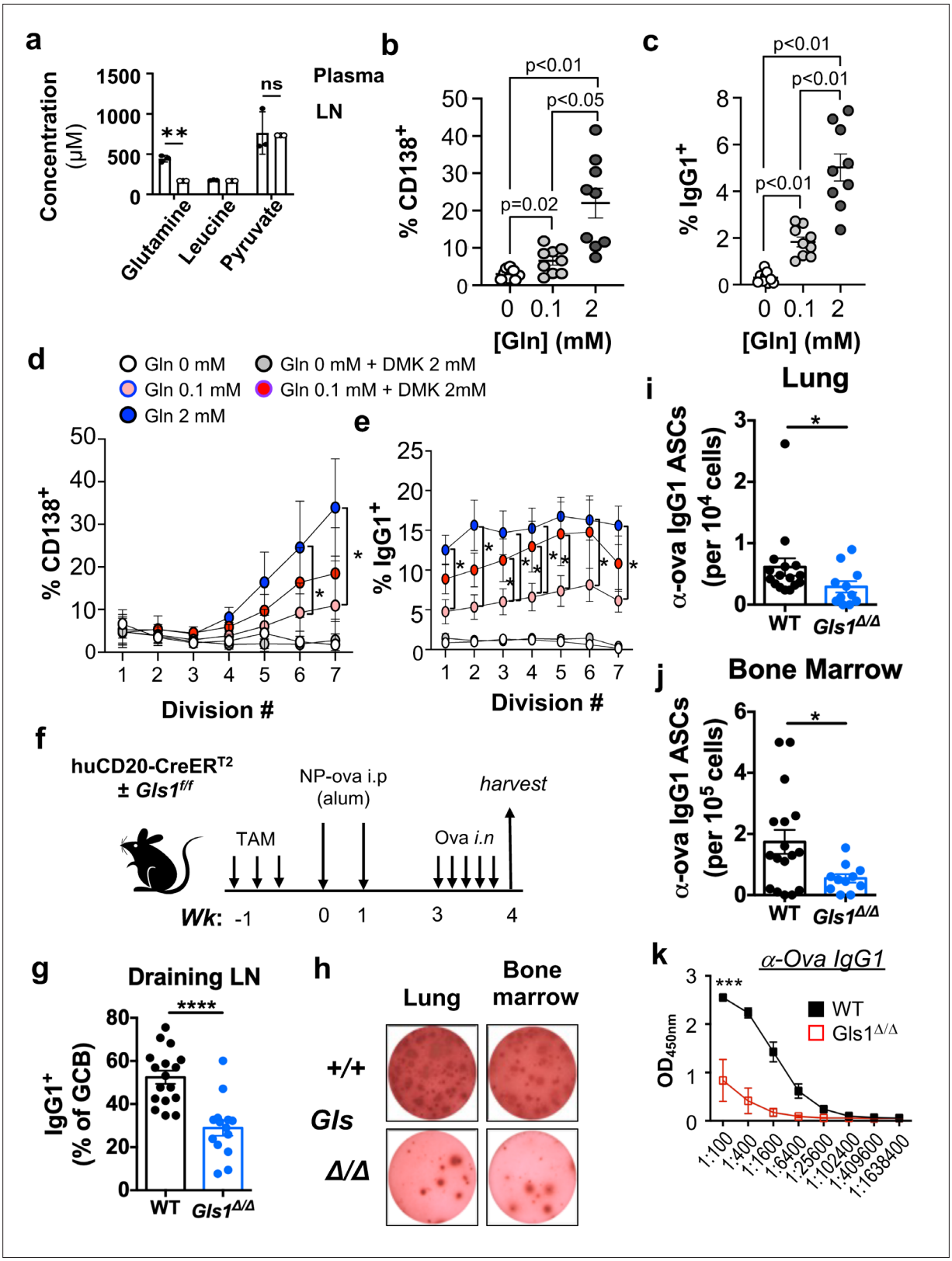


Figure 1. Glutamine and glutaminolysis promote antibody response to ovalbumin. (**a**) Reduced glutamine concentration in LN relative to the bloodstream. Shown are the results from measuring concentrations of glutamine, leucine, and pyruvate in the centrifugal eluates (***Haslene-Hox et al., 2011***; ***Sugiura et al., 2022***) of lymph nodes or plasma of mice (n=3), as described in the *Materials and methods*. (**b, c**) B cells from WT B6 mice were activated and cultured together with anti-IgM, BAFF, IL4, and IL5 in the presence of the indicated concentrations of Gln. Shown are the mean

Figure 1 continued on next page

Figure 1 continued

(± SEM) frequencies of CD138$^+$ B220^{lo} PC (**b**) and IgG1$^+$ B cells (**c**) after culture for 5 days. (**d, e**) Effects of cell-permeable α-ketoglutarate precursor, dimethyl-α-ketoglutarate (DMK), on the impaired PC differentiation and IgG class switching caused by Gln restriction. CellTrace Violet-labeled B cells were activated and cultured as in (**b**), with the addition of supplemental DMK as indicated. Shown are mean (± SEM) frequencies of % CD138$^+$ (**d**) and IgG1$^+$ B cells (**e**) within each division-counted peak. (**b–e**) Results aggregated from three biological replicate experiments. p-Values were calculated by Mann-Whitney U test. *p<0.05. Related data are presented in supplement 1 to this Figure. (**f–k**) An anti-ovalbumin Ab response is promoted by B cell expression of GLS. (**f**) Schematic of the immunization with priming and sensitization of tamoxifen-treated mice of the indicated genotypes [huCD20-CreER^{T2+} and either *Gls* +/+ (WT) or *Gls* f/f], followed at week 3 by challenges with intranasal instillations of sterile ovalbumin solution. (**g**) Mediastinal LN were collected from harvested mice and the frequencies of IgG1$^+$ events in the GL7$^+$ CD95$^+$ B cell gate were measured by flow cytometry. Each dot represents an individual mouse, with bars denoting the mean values. (**h–k**) Single-cell suspensions of lung and bone marrow were analyzed by ELISpot assays with ovalbumin-coated filters to capture secreted Ag-specific Ab detected using anti-mouse IgG1. Shown are (**h**) representative wells from the indicated sources (organ; genotype of B cells) and aggregated frequencies of anti-ova IgG1$^+$ ASCs in lung (**i**) and marrow (**j**). (**k**) Anti-ova IgG1 in sera of the mice with B cell-restricted depletion of GLS (*Gls*$^{\Delta\Delta}$) or controls, as indicated. Shown are data from ELISA with serial fourfold dilutions using individual samples from each mouse. The likelihood of each null hypothesis (no true difference between two samples) was calculated as noted in the Materials and methods (two-tailed and non-parametric testing where conditions not met for Student's t-test). *p<0.05, **p<0.01, *** p<0.001, ****p<0.0001.

The online version of this article includes the following source data and figure supplement(s) for figure 1:

Source data 1. sRaw numbers or other primary info used in preparation of figure panels.

Source data 2. Calculation modes for use of proton NMR to measure indicated metabolites.

Source data 3. Excel file as source data with raw numbers used in preparation of the graphs in ***Figure 1d***.

Source data 4. Excel file as source data with raw numbers used in preparation of the graphs in ***Figure 1d***.

Source data 5. Excel file as source data with raw numbers used in preparation of the graphs in ***Figure 1d***.

Source data 6. Excel file as source data with raw numbers used in preparation of the graphs in ***Figure 1e***.

Source data 7. Files with data used for panels g-j of ***Figure 1***.

Source data 8. Files with data used for graph of ***Figure 1k*** with anti-ova IgG1.

Figure supplement 1. Glutamine and glutaminolysis promote antibody response to ovalbumin.

Figure supplement 1—source data 1. Collection of files used for this supplement to ***Figure 1***.

Figure supplement 2. Glutamine and glutaminolysis promote antibody response to ovalbumin.

Figure supplement 2—source data 1. Raw immunoblots shown in ***Figure 1—figure supplement 2a***.

Figure supplement 2—source data 2. Raw immunoblots shown in ***Figure 1—figure supplement 2a***, labelled.

Figure supplement 2—source data 3. Raw SDS-PAGE images shown in ***Figure 1—figure supplement 2b***.

Figure supplement 2—source data 4. Raw SDS-PAGE images shown in ***Figure 1—figure supplement 2b***, labelled.

experimental conditions, glutaminolysis within B cells promoted the development of Ag-specific ASCs and an anti-protein Ab response.

Glutaminolysis is mostly dispensable for anti-NP responses yet synergizes with other metabolic needs

Mitochondrial oxidative metabolism appears to promote affinity maturation in the classic hapten-carrier model of an Ab response specific for nitrophenolic (NP) adducts (***Chen et al., 2021***; ***Urbanczyk et al., 2022***; ***Yazicioglu et al., 2023***). In contrast to the impact of *Gls* inactivation on an anti-protein response after ovalbumin inhalation (***Figures 1 and 2a-c***), the anti-NP Ab response and affinity maturation were unaffected (***Figure 2a and d–i***). Notably, however, B cell-specific inactivation of *Gls* synergized with loss of GLUT1. Thus, combining inducible B cell-specific gene targeting that restricted glucose import into B cells (***Caro-Maldonado et al., 2014***; ***Brookens et al., 2024***; ***Bierling et al., 2024***) with GLS depletion caused dramatically greater decreases in anti-Ova and anti-NP ASCs than iB inactivation of *Slc2a1* alone (***Figure 2b–i***). Combined *Gls* and *Slc2a1* inactivation had a relatively modest impact on IgM anti-NP compared to samples with *Slc2a1*$^{\Delta\Delta}$ B cells (***Figure 2g***). In contrast, a synergism was evident in the effects on circulating Ag-specific IgG1, for which B-specific inactivation of both *Gls* and *Slc2a1* dramatically compromised the humoral response, whereas GLUT1 depletion reduced anti-NP Ab to 1/2 - 1/4 levels of WT controls and a single loss-of-function mutation for *Gls* had no effect (***Figure 2g–i***). The synergism was most striking for high-affinity IgG1 (***Figure 2i***), though it also impacted all-affinity IgG1 (***Figure 2h***). The modes of eliciting Ab responses differed for ovalbumin- and NP-specific B cells, but the data indicate that the need for glutaminolysis depended on

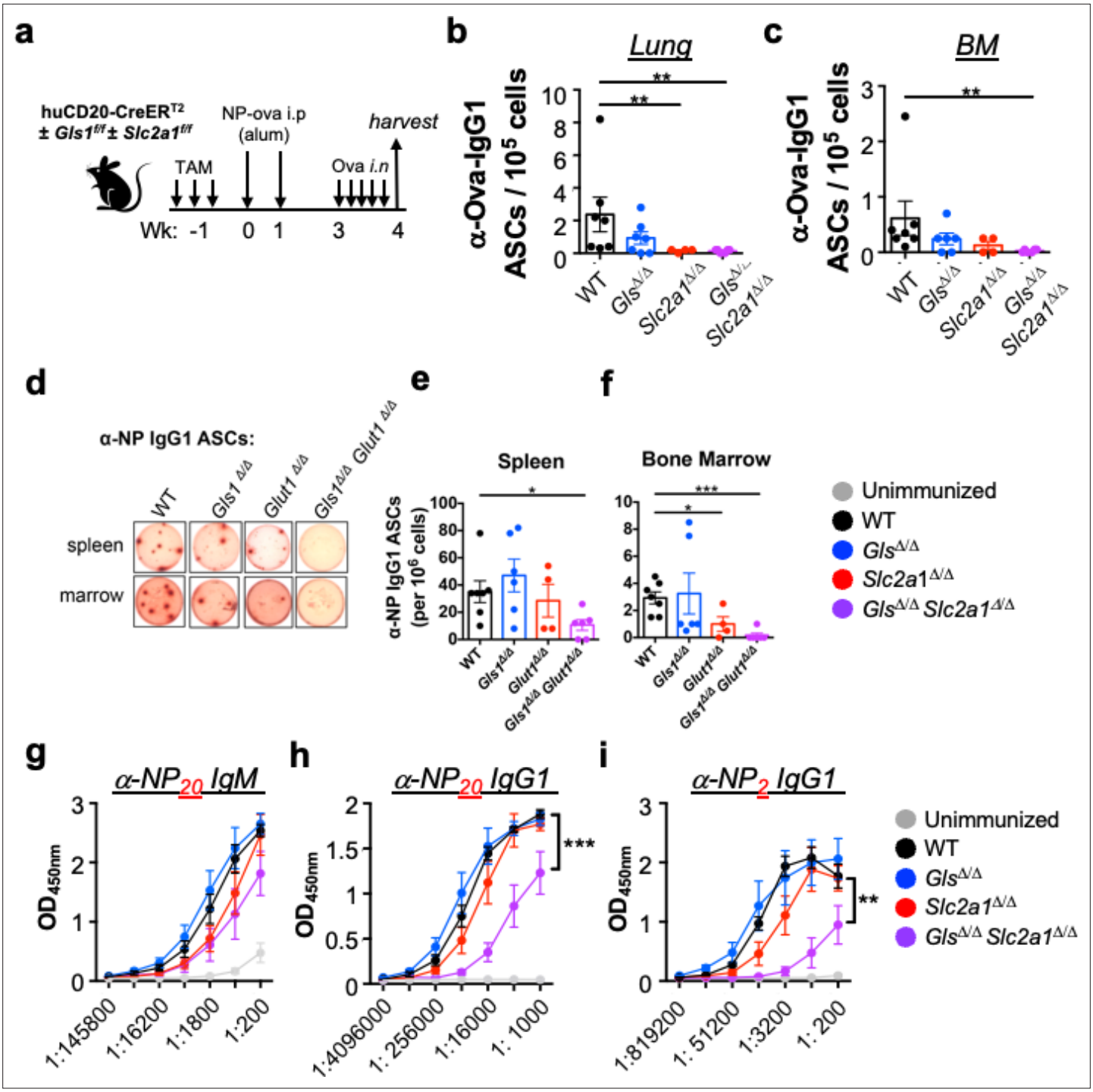


Figure 2. Glutaminolysis only conditionally supports the anti-NP Ab response. (**a**) Schematic of the immunization with priming sensitization and inhaled challenge of tamoxifen-treated mice of the indicated genotypes [huCD20-CreER^{T2+} and the indicated combinations of either *Gls* +/+ (WT) or *Gls* f/f and either *Slc2a1* +/+ (WT) or *Slc2a1* f/f], followed at week three by challenges with intranasal instillations of sterile ovalbumin solution. (**b–f**) ELISpot analyses of cells secreting IgG1 anti-ovalbumin (**b, c**) and anti-NP (**d-f**) Ab in mice of the indicated genotypes. Shown are counts from the lung suspensions (**b**), bone marrow (**c, d, f**), and spleens (**d, e**) from each individual mouse, with means (± SEMs) for the aggregate data denoted as bar graphs. (**d**) Representative ELISpot wells scoring the frequencies of IgG1 anti-NP Ab-secreting cells in spleen and marrow of mice whose B cells were converted to the indicated genotypes [wildtype (●), *Gls*$^{Δ/Δ}$ (●), *Slc2a1*$^{Δ/Δ}$ (●), and *Gls*$^{Δ/Δ}$ *Slc2a1*$^{Δ/Δ}$ (●)] after immunization and rechallenge. (**e, f**) Aggregate data with ASC counts for IgG1 anti-NP-secreting cells in spleen (**e**) and marrow (**f**). Data were pooled from two independent experiments (seven wildtype, six *Gls*$^{Δ/Δ}$, four *Slc2a1*$^{Δ/Δ}$, and six *Gls*$^{Δ/Δ}$ *Slc2a1*$^{Δ/Δ}$ mice). * p<0.05, ** p<0.01, *** p<0.001 (Mann-Whitney U test).(**g–i**). Shown are the mean

Figure 2 continued on next page

Figure 2 continued

(± SEM) absorbances of aggregated results of ELISA analyses of the IgM (**g**) and IgG1 (**h, i**) responses in the immunized mice of the two independent experiments, comparing all-affinity (**h**) to high-affinity (**i**) anti-NP, using serial threefold or fourfold dilutions when detecting IgM and IgG1, respectively.

The online version of this article includes the following source data for figure 2:

Source data 1. One tranche of a collection of data files used in preparation of ***Figure 2*** (split due to size limits).

Source data 2. Second tranche of a collection of data files used in preparation of ***Figure 2*** (split due to size limits).

Source data 3. Excel files with numerical data used in preparing graphs of ***Figure 2***.

Ag and immunization. Even for the anti-NP response, glutaminolysis within the B cells was important for their function if glucose import was restricted.

Glucose oxidation rates are several-fold higher in GC B cells than in their naive counterparts (***Brookens et al., 2024***). However, the effects of eliminating GLUT1 on a GLS-deficient background could be due to glucose usage in serine generation (***D'Avola et al., 2022***), the pentose phosphate pathway (***Brookens et al., 2024***), or glycosylation (***Lam et al., 2016***) rather than from reduced pyruvate flow into mitochondrial metabolism. Directly to interfere with pyruvate import into mitochondria for generation of acetyl-CoA, we used a previously characterized allele for inducible inactivation of *Mpc2*, a gene encoding an essential subunit of the mitochondrial pyruvate channel (***Figure 3a***; ***Zangari et al., 2020***; ***Lam et al., 2016***). Although IgG1 is conventionally a primary read-out, it is established that these immunizations can elicit IgG2c. This paralogue of human IgG1 can play particularly salient roles in control of pathogens and in auto-Ab-mediated organ damage during auto-immunity (***Cunningham et al., 2007***; ***Rubtsova et al., 2013***; ***Luan et al., 2026***). Levels of class-switched anti-NP antibodies in sera after the second immunization were modestly reduced after inducible *Mpc2* targeting in B cells (***Figure 3b***; ***Figure 3—figure supplement 1a***), as were the concentrations of anti-NP Ab after the boost and the ratio of high- to all-affinity Ab (***Figure 3c***; ***Figure 3—figure supplement 1b, c***), one aspect of affinity maturation. Whereas GLS depletion had no effect on its own, the combined loss-of-function synergized and dramatically reduced Ag-specific IgM (***Figure 3—figure supplement 1b***) and several switched isotypes (***Figure 3b and c***; ***Figure 3—figure supplement 1a***). The capacity to produce a spectrum of Ab with higher affinities after secondary immunization was reduced further (***Figure 3c–e***), and high-affinity IgG2c anti-NP in mice with doubly deficient B cells was ~0.02 x controls, while the all-affinity was ~1/8th of the control values (***Figure 3—figure supplement 1a***). The disruption of glutaminolysis in B cells reduced their capacity to yield anti-NP IgG1 prior to secondary immunization ("boost"), an impact most striking for high-affinity Abs (***Figure 3d and e***; ***Figure 3—figure supplement 1d, e***). Moreover, compound loss of function yielded dramatically fewer cells secreting high-affinity anti-NP Ab (***Figure 3f***; ***Figure 3—figure supplement 2a, b***). Consistent with decreased proliferation in vivo (***Figure 3—figure supplement 2c***), GC-phenotype B cells (GCB) were reduced as well (~1/2 control numbers) (***Figure 3—figure supplement 2d***, supplement 3). In contrast to our findings with conditional targeting of *Slc2a1* in B cells, in which a substantial degree of counterselection was evident (***Brookens et al., 2024***), the mRNA encoding both *Gls* and *Mpc2* were far lower in flow-sorted GC B cells (***Figure 3—figure supplement 2e, f***). Although the magnitude of overall decrease in GC B cells was modest and probably less than the underrepresentation of ASCs producing anti-NP Ab (***Figure 3f***), the frequencies of NP-binding GC B cells were lower when *Gls* was disrupted (***Figure 3—figure supplement 3e***). Although the genetic impact on cellular metabolism was restricted to B cells, substantial decreases were measured for $CD4^+$ T cells of Tfh- or GC-Tfh-phenotype (***Figure 3—figure supplement 4a, b***). We conclude that glutaminolysis in B cells promotes GC B cell numbers, function, as well as affinity maturation, the production of Ag-specific ASCs, and levels of Ag-specific Ab.

We next tested how these losses of function impact a recall process by delaying tamoxifen treatments until several weeks after the priming immunization, with the initiation of deletion followed by the second immunization and harvest (***Figure 3g***). In this setting where the primary response from a pre-immune repertoire was unperturbed, we once again observed that *Gls* gene inactivation reduced Ab responses primarily when *Mpc2* also was disrupted (***Figure 3h***; ***Figure 3—figure supplement 4c–e***). High-affinity anti-NP Ab of several switched isotypes were drastically reduced: IgG1 to <1/4 of control values (***Figure 3h***), with IgG2c and IgA almost undetectable (***Figure 3—figure supplement 4c–e***). Moreover, frequencies of anti-NP ASCs among splenocytes were lower (***Figure 3—figure***

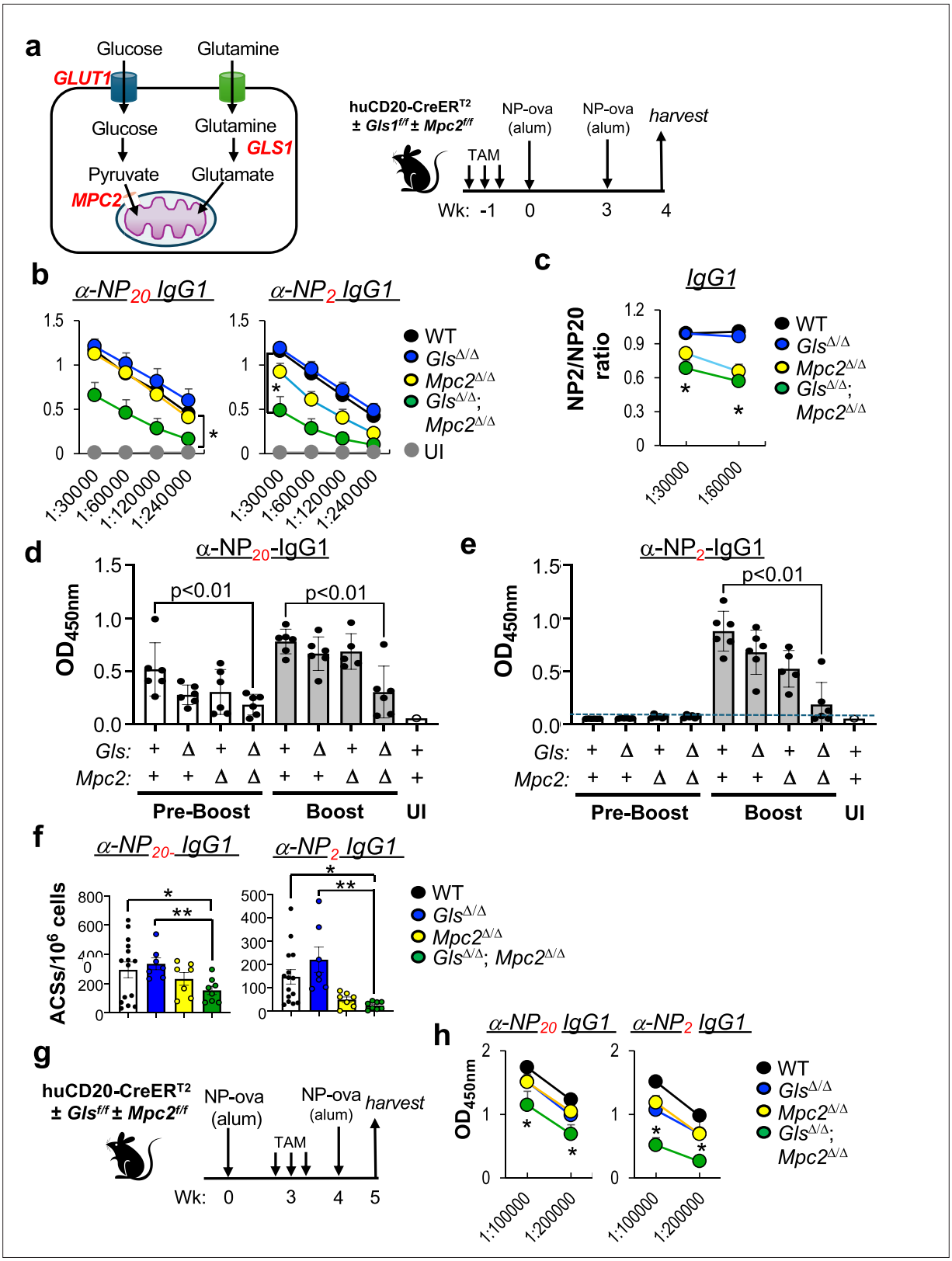


Figure 3. Synthetic auxotrophy – glutaminase support of anti-NP response is dependent on mitochondrial pyruvate channel subunit 2. (**a**) Schematic of the immunization with priming and a recall boost of mice of the indicated genotypes [huCD20-CreER^{T2+} and the indicated combinations of either *Gls* +/+ (WT) or *Gls* f/f and either *Mpc2* +/+ (WT) or *Mpc2* f/f], treated with tamoxifen prior to the initial immunization. (**b, c**) Results of serological analyses performed on sera from the time of harvest. Shown are the mean (± SEM) absorbances measured in ELISA for detection of all- and high-affinity Abs

Figure 3 continued on next page

Figure 3 continued

(α-NP_{20} and α-NP_2, respectively) of the IgG1 (**b**) and the relative strengths of affinity maturation (**c**). Impacts of altered metabolic pathways in B cells on relative extents of affinity maturation in the recall responses are shown as mean ratios of absorbances for high- (NP_2) / all-affinity (NP_{20}) ELISA at two serum dilutions for the IgG1 isotype. The analogous serologic measurements of IgM and IgG2c anti-NP Ab are shown in ***Figure 3—figure supplement 1***. (**d, e**) Altered glutaminolysis and pyruvate import collaborate in support of the response to primary immunization as well as the Ab after a secondary immunization ('boost'). All- and high-affinity anti-NP IgG1 was measured in the sera of mice whose B cells were converted to the indicated genotypes by tamoxifen injections and then immunized as in (**a**). Shown are mean (± SEM) absorbances for (**d**) all- (αNP_{20}) and high- (αNP_2) IgG1 at a single dilution of sera before ('Pre-Boost') and a week after ('Boost') the second immunization. Data represent three temporally distinct cohorts, each including two mice of each of the four genotypes. Probabilities of the null hypothesis applying (P values) for differences in pairwise comparisons are indicated. (**f**) Shown are mean (± SEM) frequencies of splenocytes producing IgG1 anti-NP Ab of the indicated affinities at harvest after the booster immunization as in (**a**), with genotypes as shown and each dot representing an individual mouse. Data on IgG2c and IgM isotypes are presented in ***Figure 3—figure supplement 2***. (**b–f**) Results are aggregated from four temporally separate immunization experiments with mice of each genotype, totaling eight individual controls [(WT, i.e. only $CreER^{T2+}$) (●)] and eight mice with each type of induced B cell type-specific deletion [$Gls^{\Delta/\Delta}$ (●), $Mpc2^{\Delta/\Delta}$ (●), and $Gls^{\Delta/\Delta}$ $Mpc2^{\Delta/\Delta}$ (●) genotypes]. Related and additional results – affinity maturation (NP_2/NP_{20} ratios), frequencies of GC B cells and the NP-binding population therein, MBCs, BrdU uptake rates in GC B cells, as well as *Gls* and *Mpc2* mRNA – are presented in ***Figure 3—figure supplements 1–3***. (**g, h**) Functional requirements for GLS and MPC2 in B cells in a recall phase after secondary immunization. (**g**) Schematic of the priming immunization without deletion of the conditional alleles, followed by tamoxifen injections ~3 weeks later, and only then a recall boost of mice of the indicated genotypes [huCD20-$CreER^{T2+}$ and the indicated combinations of either *Gls* +/+ (WT) or *Gls* f/f and either *Mpc2* +/+ (WT) or *Mpc2* f/f]. (**h**) Shown are serologies of the all- and high-affinity IgG1 anti-NP Ab elicited by a boost when Cre activation was initiated only after the primary response. Results are aggregated from three temporally separate immunization experiments with mice of each genotype, totaling nine individual controls [(WT, i.e. only $CreER^{T2+}$) (●)] and nine mice with each type of induced B cell-specific deletion [$Gls^{\Delta/\Delta}$ (●), $Mpc2^{\Delta/\Delta}$ (●), and $Gls^{\Delta/\Delta}$ $Mpc2^{\Delta/\Delta}$ (●) genotypes]. ***Figure 3—figure supplements 4 and 5*** show additional results, with IgM, IgG2c, and IgA isotypes; frequencies of ASCs, total and NP-binding GC B cells as well as Tfh / GC-Tfh cells.

The online version of this article includes the following source data and figure supplement(s) for figure 3:

Source data 1. Excel file with the numerical data from ELISA measurements used to graph ***Figure 3b***.

Source data 2. Excel file with the numerical data used to graph ***Figure 3c*** based on ratios of values in ELISA measurements.

Source data 3. Excel file with the numerical data from ELISA measurements used to plot dots in ***Figure 3d***.

Source data 4. Excel file with the numerical data from ELISA measurements used to plot dots in ***Figure 3e***.

Source data 5. Excel file with the numerical data from ELISpot measurements used to plot ***Figure 3f***.

Source data 6. Excel file with the numerical data from ELISA measurements used to plot dots in ***Figure 3***.

Figure supplement 1. Synthetic auxotrophy – glutaminase support of anti-NP response is dependent on mitochondrial pyruvate channel subunit 2.

Figure supplement 1—source data 1. Excel with numberical data for plotting ELISA results of ***Figure 3—figure supplement 1a***.

Figure supplement 1—source data 2. Excel with numberical data for plotting ELISA results of ***Figure 3—figure supplement 1b***.

Figure supplement 1—source data 3. Excel with numberical data for plots of ***Figure 3—figure supplement 1c*** as calculated from ELISA in 1a, 1c.

Figure supplement 1—source data 4. Excel with numbers for the dot plots in which ratios of high-affinity to all-affinity IgG1 anti-NP were calculated based on ELISA of ***Figure 3***.

Figure supplement 1—source data 5. Excel with numbers used for the increased absorbances in ELISA performed with sera for each mouse (IgG1 after - before the boost / 2nd immunization).

Figure supplement 2. Synthetic auxotrophy – glutaminase support of anti-NP response is dependent on mitochondrial pyruvate channel subunit 2.

Figure supplement 2—source data 1. Excel file with the raw data used to plot bar and dots graph of the numbers of Ab-secreting cells in ***Figure 3—figure supplement 2a***.

Figure supplement 2—source data 2. Excel file with the raw data used to plot bar and dots graph of the numbers of IgM Ab-secreting cells in ***Figure 3—figure supplement 2b***.

Figure supplement 3. Synthetic auxotrophy – glutaminase support of anti-NP response is dependent on mitochondrial pyruvate channel subunit 2.

Figure supplement 3—source data 1. Excel tabulation of the dot graph in ***Figure 3—figure supplement 3b***, showing prevalence of GC-phenotype B cells in the indicated flow cytometry 'gate'.

Figure supplement 3—source data 2. Excel tabulation of the dot graph in ***Figure 3—figure supplement 3d*** showing prevalence of GC-phenotype B cells in the indicated flow cytometry 'gate'.

Figure supplement 3—source data 3. Excel tabulation of the dot graph in ***Figure 3—figure supplement 3d***, showing prevalence of GC-phenotype B cells in the indicated flow cytometry 'gate'.

Figure supplement 3—source data 4. Excel tabulation of the dot graph in ***Figure 3—figure supplement 3e***, showing prevalence of NP-binding event among GC-phenotype B cells in the indicated flow cytometry 'gate'.

Figure supplement 4. Glutamine and pyruvate metabolism in B cells affects their support to follicular helper T cells.

Figure supplement 4—source data 1. Excel with two tabs, each with numerical data used to graph dot plots presented in ***Figure 3—figure***

Figure 3 continued on next page

Figure 3 continued

supplement 4b.

Figure supplement 4—source data 2. Excel with two tabs, each with numerical data used to graph dot plots of ELISA results presented in ***Figure 3—figure supplement 4c***.

Figure supplement 4—source data 3. Excel with two tabs, each with numerical data used to graph dot plots of ELISA results presented in ***Figure 3—figure supplement 4d***.

Figure supplement 4—source data 4. Excel with two tabs, each with numerical data used to graph dot plots of ELISA results presented in ***Figure 3—figure supplement 4e***.

Figure supplement 5. Synthetic auxotrophy – glutaminase support of splenic production of anti-NP ASCs is enhanced by mitochondrial pyruvate channel subunit 2.

Figure supplement 5—source data 1. Excel file with numbers of ASCs used to plot dots in ***Figure 3—figure supplement 5a***.

Figure supplement 5—source data 2. Excel file with numbers of ASCs used to plot dots in ***Figure 3—figure supplement 5b***.

Figure supplement 5—source data 3. Excel file with numbers of IgG2c anti-NP ASCs used to plot dots in ***Figure 3—figure supplement 5c***.

Figure supplement 5—source data 4. Excel file with numbers of ASCs used to plot dotsin ***Figure 3—figure supplement 5d***.

Figure supplement 5—source data 5. Excel file with numbers of high-affinity IgM anti-NP ASCs used to plot dots in ***Figure 3—figure supplement 5e***.

Figure supplement 5—source data 6. Excel file with numbers of high-affinity IgG2c anti-NP ASCs used to plot dots in ***Figure 3—figure supplement 5f***.

Figure supplement 5—source data 7. Excel file with frequencies of NP-binding GC B cells used to plot dots in ***Figure 3—figure supplement 5g***.

supplement 5a–f). Since high-affinity, class-switched (IgG or IgA) Ab are undetectable 1 week after a primary immunization, we infer from these results that the rapid generation of the ASCs producing these Ab required glutaminolysis and pyruvate import. The splenic ASC pool and high-affinity IgG anti-NP Ab in sera 7 d after a recall challenge can arise from two main sources. Ag-specific MBC can rapidly differentiate into PC without need GC re-entry (***Mesin et al., 2020***; ***Kometani et al., 2013***). Some GC B cells in persisting follicles may receive additional Ag exposure after secondary immunization, despite the Ab-specific Ab (***Mesin et al., 2026***). In several models, however, re-activation of MBCs that directly differentiated into PCs after the second immunization was the primary source of the Ab (***Leach et al., 2019***; ***Schiepers et al., 2024***; ***Wong et al., 2020***; reviewed in ***Victora and Nussenzweig, 2022***; ***Inoue and Kurosaki, 2024***). Nonetheless, some of the effects of GLS and the MPC on Ab levels and ASC generation in these experiments with delayed gene inactivation may be due to impairment within the GC B cells. Irrespective of this latter possibility, the findings reveal a B cell-intrinsic process that acts well after an initial priming immunization and promote both affinity selection and differentiation toward a PC fate through the collaboration of pyruvate influx rate and glutaminolysis.

Synthetic auxotrophy of progressively increased respiration and PC differentiation

Glutaminolysis and mitochondrial pyruvate import each can be inhibited by a well-characterized pharmaceutical compound – CB839 (***Johnson et al., 2018***) and UK5099 (***Zangari et al., 2020***; ***Lam et al., 2016***), respectively. We tested the effect of these agents – in combination, or each one singly-on physiology and differentiation of B cells activated via CD40. CB839 reduced the production of $CD138^+$ progeny (***Figure 4a and b***), ASC (***Figure 4c and d***), and Ab (***Figure 4e***). Glutaminase inhibition substantially reduced production of $CD138^+$ plasmablasts/PCs when B cells were co-activated with anti-IgM along with CD40 cross-linking, and co-inhibition of with CB839 and UK5099 further reduced differentiation (***Figure 4—figure supplement 1a, b***). In part, this effect of glutaminase inhibition was due to decreased efficiency of dividing (***Figure 4—figure supplement 1c***), which was accompanied by lower cell numbers (***Figure 4—figure supplement 1d***) with a more modest effect on viability (***Figure 4—figure supplement 1e***). Consistent with its ability to inhibit glutaminase, this agent decreased intracellular glutamate and the calculated glutaminolysis rate while increasing the glutamine pool (***Figure 4—figure supplement 2a–c, e***). On its own, UK5099 had no effect on development of $CD138^+$ cells, yet addition of UK5099 to CB839 substantially intensified the inhibition of ASC generation and Ab production. Of note, UK5099 reduced neither glutamine nor glutamate, yet substantially reduced intracellular alanine, which is generated in mitochondria by glutamate-pyruvate

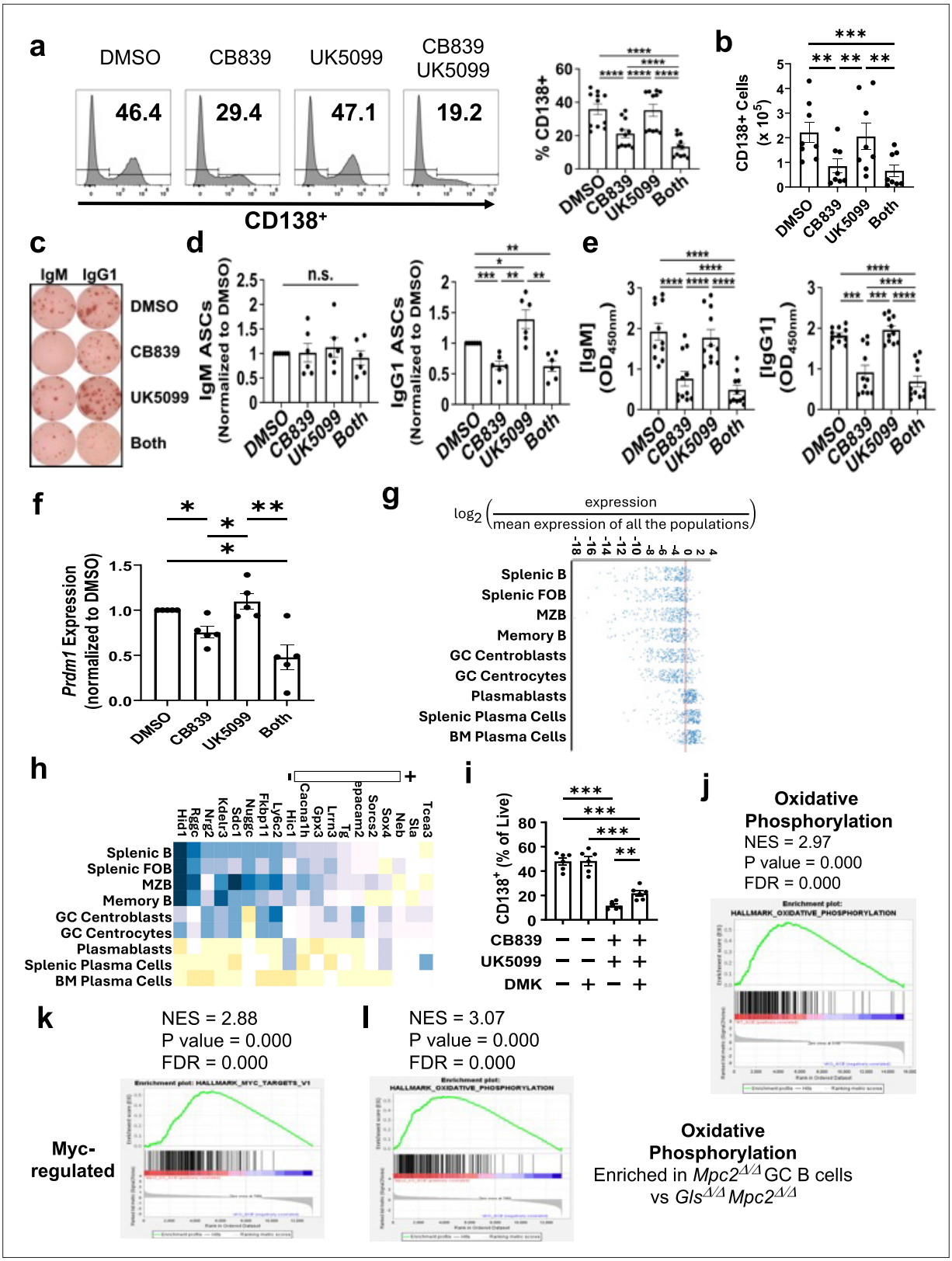


Figure 4. GLS and MPC2 collaborate in supporting progression to plasma cell (PC) development. (**a**) B cells were activated and cultured under conditions promoting PC differentiation in the presence of the indicated combinations of vehicle (DMSO) or inhibitors of GLS (CD839) and the MPC (UK5099). Shown are representative histograms from flow cytometric analyses of CD138 within the live cell gate, with inset numbers denoting the %CD138$^+$. The bar graph shows the mean (± SEM) results for generation of CD138$^+$ cells under each treatment condition, pooling data from three

Figure 4 continued on next page

Figure 4 continued

temporally independent experiments, each with three to five independent B cell pools purified from separate mice (each dot represents a distinct sample). (**b**) Shown are the mean (± SEM) calculated numbers of PC generated in temporally independent replica experiments with a total of eight independent B cell pools cultured in vitro in (**a**). (**c**) Representative ELISpot results measuring the frequencies of IgM- and IgG1-secreting PC, as indicated, produced in the differentiation cultures under each treatment condition. (**d**) Bar graphs with mean (± SEM) ELISpot results pooled from the replicate experiments illustrated in (**c**), with each dot representing an individual sample. Shown are data normalized to the vehicle (DMSO) control for each set of cultures using an individual B cell pool. (**e**) Bar graphs show the mean (± SEM) absorbance values from ELISA measurements of IgM and IgG1 secreted into the media during the cultures as in (**b**). Additional data quantifying ASCs are presented in ***Figure 4—figure supplement 1a***. (**f**) *Prdm1* gene expression promoted by GLS and MPC2. B cells were activated and cultured as above, but harvested after 3.5 d culture in BAFF, IL-4, IL-5, and the indicated inhibitor(s) or vehicle followed by qRT2-PCR to quantitate *Prdm1* RNA encoding Blimp1. Shown are the results from four biologically independent mouse pools, B cell purifications and cultures, with the *Prdm1*-encoded RNA then normalized in each experiment to the level in the vehicle (DMSO) control (in each sample, relative to the averaged C_T values of cyclophilin A and GAPDH). (**g, h**) Global gene expression identifies PC identity as a main target of synthetic auxotrophy. Using three biologically independent replicate pools for each condition, RNA-seq was performed with the B cells cultured as in (**f**). Enriched genes identified by DESeq2 comparison were analyzed using the MyGeneset tool from ImmGen. (**g**) Genes enriched in vehicle treated cultures compared to cultures treated with both CB839 and UK5099 are shown as a W-plot with defined stages for mature B cells and PC indicated. (**h**) Genes enriched in CB839-treated cultures compared to cultures treated with both CB839 and UK5099 are shown as a heatmap of z-scored relative expression, with specific gene identities and defined stages for mature B cells and PC indicated. (**i**) Metabolic mitigation of the block imposed by synthetic auxotrophy. Graphs of aggregate results from six biologically independent B cell preparations (two biological replicates in each of three independent experiments, presented as in (**a**), are shown for differentiation assays performed with B cells purified, activated, and cultured as in (**a**), except that the cell permeable αKG analogue DMK was added as indicated. (**j–l**) Gene set enrichment analyses (GSEAs) were performed on RNA-seq data generated using RNA from flow-purified GC B cells and hallmark gene sets of the Mouse Molecular Signatures Database. $CreER^{T2}$ -transgenic mice of each of the four genotypes (*Gls* +/+or f/f; *Mpc2* +/+or f/f) were immunized with SRBC after being treated sequentially with tamoxifen to activate huCD20-$CreER^{T2}$ as diagrammed in ***Figure 3a***. One week after immunization, RNA was isolated from viable GC-phenotype B cells purified by flow sorting, as well as from IgD^+ B cells. RNA-seq data were quality-controlled, processed, and organized into GSEAs as described in the Methods. Shown is a selected subset of analyses with high normalized enrichment scores (NES) for the indicated gene sets (**j**) oxidative phosphorylation (WT vs $Gls^{\Delta\Delta}$, $Mpc2^{\Delta\Delta}$ GC B cells); (**k**) regulated by c-Myc ($Mpc2^{\Delta\Delta}$ vs $Gls^{\Delta\Delta}$, $Mpc2^{\Delta\Delta}$ GC B cells); (**l**) oxidative phosphorylation ($Mpc2^{\Delta\Delta}$ vs $Gls^{\Delta\Delta}$, $Mpc2^{\Delta\Delta}$ GC B cells). Additional GSEA and other data are in ***Figure 4—figure supplement 5***).

The online version of this article includes the following source data and figure supplement(s) for figure 4:

Source data 1. Data of ***Figure 4a***.

Source data 2. Data in support of relative IgM production in ***Figure 4e***.

Source data 3. Data in support of relative IgG1 production in ***Figure 4e***.

Source data 4. Data in support of the time point for analyses of levels of mRNA encoding Blimp-1 during differentiation of activated B cells into PB/PC for ***Figure 4f***.

Source data 5. Data for individual replicate experiments measuring relative levels of the mRNA encoding Blimp-1 under various conditions, ***Figure 4f***.

Figure supplement 1. Glutaminolysis, especially in concert with mitochondrial pyruvate import, promotes proliferation, viability, and differentiation of anti-IgM-stimulated B cells.

Figure supplement 1—source data 1. Excel with numerical data on effects of metabolism inhibitors on development of CD138+ PB/PC presented in dot plots of replicate experiments' results in ***Figure 4—figure supplement 1b***.

Figure supplement 1—source data 2. Excel with numerical data on effects of metabolism inhibitors on division efficiencies presented in dot plots of replicate experiments' results in ***Figure 4—figure supplement 1c***.

Figure supplement 1—source data 3. Excel with quantitative data on replication series for numbers of viable B cells recovered at ends of cultures, as in ***Figure 4—figure supplement 1d***.

Figure supplement 1—source data 4. Excel file with numerical data on prevalence of viable B cells in replicate experiments whose results are plotted in ***Figure 4—figure supplement 1e***.

Figure supplement 2. Metabolite evidence of the impact of CB839 on glutaminolysis and mitochondrial metabolism in activated B cells.

Figure supplement 2—source data 1. Source data for metabolomic analyses presented in ***Figure 4—figure supplement 2***.

Figure supplement 3. Impacts of glutaminolysis, alone or in concert with mitochondrial pyruvate import, on differentiation vs secretory function of B lymphoblast-derived plasma cells.

Figure supplement 3—source data 1. Data on effects of agents on relative frequencies of cells differenrtiated to produce IgG1.

Figure supplement 4. On the relationship between proliferation effects and differentiation efficiency of B cells treated with CB839, alone or in concert with hydroxychloroquine.

Figure supplement 5. Altered gene expression of metabolically reprogrammed B cells Additional data relating to the analyses of RNA-seq results with flow-purified GC B cells (controls versus those with disruption of *Gls*, *Mpc2*, or both; ***Figure 4j–l***; ***Figure 6a–c***).

transaminase 2 (GPT2) conversion of glutamate and pyruvate to alanine and αKG (***Figure 4—figure supplement 2d***). Further, the frequencies of ASCs and spot sizes were substantially reduced when metabolism was inhibited only during the differentiation phase, followed by washout of the inhibitors (***Figure 4—figure supplement 3***). These data indicate that glutaminolysis and mitochondrial pyruvate import promote the differentiation process. Nonetheless, results from applying inhibitors only during the ELISpot culture, that is after 4 days of differentiation in vitro, suggest that glutaminolysis also non-redundantly supports the synthesis and/or secretion of Ab (***Figure 4—figure supplement 3b, d***).

Progression from B cell activation to the differentiation of plasmablasts and PCs requires several rounds of cell cycling and a division-counting mechanism (***Barwick et al., 2016***). When the frequency of $CD138^+$ progeny was measured as a function of division number, the results showed that CB839 reduced the capacity to become CD138-positive at equal divisions (***Figure 4—figure supplement 4a–d***). Moreover, whereas UK5099 on its own did not reduce differentiation efficiency at equal divisions, its addition intensified the inhibitory effect of CB839 (***Figure 4—figure supplement 4a–d***). Recent work with profound B cell-depletion therapy in chronic autoimmune disease indicates that disease activity depends on continual production of new auto-Ab-producing cells (***Müller et al., 2024***, reviewed in ***Taubmann et al., 2024***). Hydroxychloroquine (HCQ) is the standard of care in SLE; while effective, it incompletely reduces pathogenic auto-Ab concentrations and disease activity, and often is not sufficient (***Olsen et al., 2013***). We explored the interplay between HCQ and CB839 (glutaminase inhibition), alone or along with UK5099. Strikingly, whereas HCQ alone slightly increased the $\%CD138^+$ at each division and overall, the addition of HCQ to metabolic inhibition caused more substantial reductions in PC differentiation (***Figure 4—figure supplement 4a–d***).

Levels of *Prdm1* mRNA, which encodes a transcription factor that determines PC fate and identity [reviewed in ***Boothby et al., 2019***; ***Ripperger and Bhattacharya, 2021***], were lower in inhibitor-treated cells at a time in the cultures when the $CD138^+$ population just started to develop (***Figure 4f***). This finding is consistent with an effect on differentiation beyond simple division-counting and with the pattern of results with metabolic inhibition. Moreover, analyses of cell-type modules in RNA-seq data from B lymphoblast cultures at this inflection point yielded evidence that the main systemic impact of combined inhibition was on plasmablast–PC gene expression programs (***Figure 4g and h***). We further found that DMK, the cell-permeable αKG precursor, partially reversed the inhibitory effects of CD839 and UK5099 on B cell differentiation to a $CD138^+$ plasmablast/PC status (***Figure 4i***). While not the entire mechanism, these findings indicate that αKG generation via glutaminolysis promotes PC differentiation.

The serological data highlight an impact on affinity maturation of class-switched Ab after a secondary immunization. T cell help drives greater proliferation of both extrafollicular- and GC-B cell-derived plasmablasts that bore higher-affinity BCR (***MacLean et al., 2025***; ***Chan et al., 2009***), but the findings (***Figure 3b and c***; ***Figure 3—figure supplement 2c, d***; ***Figure 3—figure supplement 3***) demonstrate effects on GC B cells. Since in vitro systems cannot faithfully recapitulate GC B cell physiology, we performed RNA-seq analyses of flow-purified GC B cells. Immunization with SRBC was performed after B cell type-specific gene inactivation was induced by tamoxifen injections into subjects of each genotype, including matched controls ($CreER^{T2}$ transgenics with +/+ alleles at the *Gls* and *Mpc2* loci). The analyses of GC-phenotype B cells harvested a week after immunization consistently showed major reductions in the mRNA encoded by the targeted genes (*Mpc2; Gls*), indicating both that deletion of the alleles flanked by loxP sites ('floxed', designated as 'f') was efficient and that the GC were not dominated by selective outgrowth of the B cells that retained functional genes (***Figure 3—figure supplement 2f, g***). Gene set enrichment analyses (GSEA) of the impact of GLS on the relative RNA levels in GC B cells highlighted modules for the interconnected functions of Myc-regulated genes, those connected to mTOR signaling and oxidative metabolism (oxidative phosphorylation; fatty acid [FA] oxidation; ***Figure 4j–l***; ***Figure 4—figure supplement 5***). Moreover, the abnormal metabolism led to reduced expression of RNAs linked to proliferation (E2F-responsive genes and those associated with the cell cycle G2-M transition; ***Figure 4—figure supplement 5a–c***). These effects could be discerned when comparing $Gls^{\Delta\Delta}$ B cells to $CreER^{T2}$, +/+ controls but effects were heightened when *Mpc2* inactivation was compared to $Mpc2^{\Delta\Delta}$, $Gls^{\Delta\Delta}$ samples or in comparing doubly-deficient B cells to WT controls (***Figure 4—figure supplement 5a–c***).

The gene modules pointed to proliferation, c-Myc (a central mediator of metabolic reprogramming), and oxidative metabolism. Oxidative metabolism is vital for PC differentiation (***Price et al.,***

2018). Accordingly, we measured respiration by B lymphoblasts of each genotype on 2 successive days after activation and culture in conditions promoting development into ASC. Of note, rates of mitochondrion-dependent oxygen consumption by WT cells quadrupled between days 1 and 2 after mitogenic stimulation (***Figure 5a–d***). Consistent with the GSEA data, the increased respiration was blunted in GLS-deficient B cells (***Figure 5a and b***). In addition, the inactivation of *Mpc2*, while not affecting respiration on its own, further reduced both the absolute rate and the capacity to increase this core mitochondrial function during the second day when GLS was deficient (***Figure 5a and b***). To explore if these effects were attributable either to abnormal naive B cells prior to stimulation, or simply to a failure to provide sufficient substrates to the mitochondria, we added CB839 or UK5099 to cultures of normal B cells after activation but performed the metabolic flux assays in the absence of inhibitors. Strikingly, the impacts on respiration caused by pharmacological inhibition initiated at the time of B cell activation matched those obtained using genetic loss of function (***Figure 5c and d***). Further consistent with altered mitochondrial metabolism, the inhibition of glutaminolysis also impacted the acetyl-carnitine/ratio that is central to the provision of substrates for FA oxidation, with reduced L-carnitine and increased acetyl-carnitine as well as computationally inferred rates of FA oxidation (***Figure 4—figure supplement 2h–j***).

Rates of extracellular acidification rates (ECAR) were measured to test if B lymphoblasts compensated for the reduced respiration by increasing 'aerobic glycolysis' – the hallmark of which would be to generate and excrete lactate from pyruvate. Targeting glutaminolysis led to striking decreases in ECAR that were even greater when in concert with interference with the MPC (***Figure 5e and f***). These decreases indicate that the interference with glutaminolysis broadly reprograms metabolism in the activated B cells. Although activated B cells perform FA oxidation (***Weisel et al., 2020***; reviewed in ***Boothby et al., 2022***), the inhibitors decreased steady-state ATP concentrations in the CD40-activated lymphoblasts (***Figure 5g***). Of note, the main cause of these decreases appeared to be interference with the capacity of B cells to increase their respiratory capacity during growth (***Figure 5h***) rather than the modest impact of acute inhibition of glutaminolysis and pyruvate import in blasts cultured in the absence of inhibitors during 2 d prior to adding inhibitors (***Figure 5i***). The reduced respiration, lower signals from TMRE staining (***Figure 5j***), together with normal signal after MitoTracker Green staining and qPCR for mitochondrial DNA content (***Figure 5—figure supplement 1a, b***), indicate that decreased respiration was linked to a reduction in mitochondrial membrane potential rather than a failure to increase mitochondrial mass or DNA. This decrease in turn was associated with an increase in reactive oxygen species (ROS) (***Figure 5k***).

Metabolic regulation of interferon cytokine receptor responsiveness

To gain further insight into molecular consequences of synthetic auxotrophy, we analyzed how *Mpc2* gene inactivation affected GLS-depleted GC B cells using the RNA-Seq data. Surprisingly, a Jak-STAT3 signature was reduced not only in GC B cells deficient GLS and MPC2 but also in the comparison of $Mpc2^{\Delta\Delta}$ to combined loss of function (***Figure 6a***; ***Figure 4—figure supplement 5a***). IL-21R, acting in large part via STAT3, is crucial for PC differentiation (***Ozaki et al., 2002***; ***Ettinger et al., 2005***; ***Avery et al., 2010***; ***Rodríguez-Bayona et al., 2013***). Cytokine receptors activate STAT3 via Jak1-mediated tyrosine phosphorylation (***Asao et al., 2001***). Of note, ROS can alter STAT3-dependent gene transcription either directly or through increasing reactive nitrogen species followed by S-nitrosylation of signaling proteins such as STAT3 (***Li et al., 2010***; ***Kim et al., 2014***; ***Butturini et al., 2020***). We found that the tyrosyl phosphorylation of Jak1 and STAT3 stimulated by IL-21 treatment of activated B cells was attenuated in cells cultured in CB839 and UK5099 (***Figure 6b***).

We next tested for evidence that the decreased effectiveness of coupling IL-21 stimulation with induction of P-STAT3 when metabolic pathways were impeded has functional significance. As noted above (***Figure 1d and e***), generation of plasmablasts and PCs includes a division-counting process (***Barwick et al., 2016***). Thus, outputs of CD138 progeny depend on both proliferation and on the efficiency of converting gene expression programs within tranches of cells that have divided a set number of times. Accordingly, we assayed the efficiency of generating $CD138^{+}$ cells from a naive pool of splenic B cells with and without addition of exogenous IL-21 after activation. In the absence of inhibitors, IL-21 far more substantially increased the partitioning of CTV between progeny cells in such cultures (***Figure 6c and d***). In sharp contrast, this cytokine increased the division barely if at all when cultures included CB839, alone or especially in combination with UK5099 (***Figure 6c and d***).

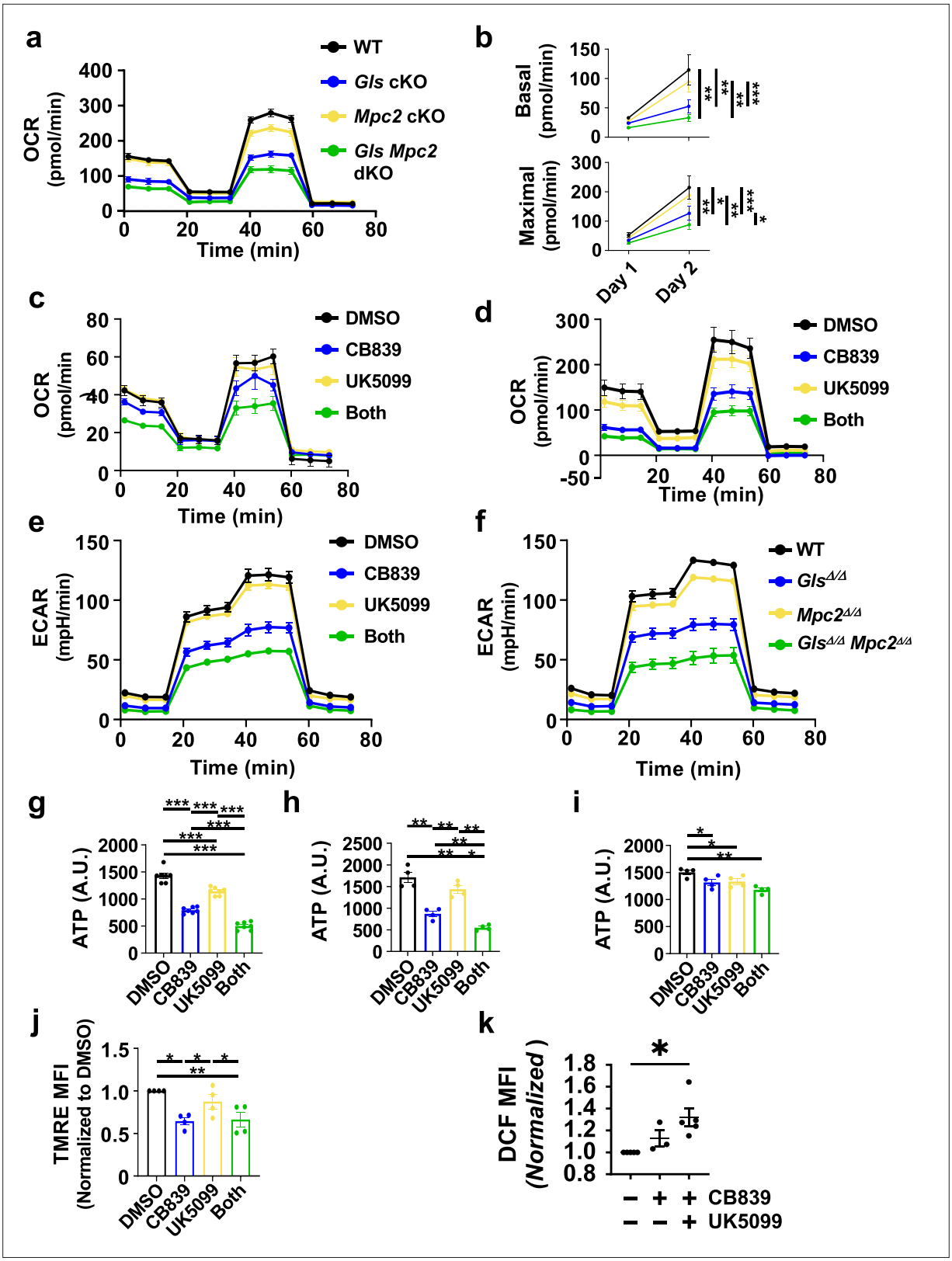


Figure 5. Synthetic auxotrophy of B cell metabolism that supports a progressive post-activation increase in mitochondrial respiration. (**a**) Pools of purified B cells from WT mice or those with the indicated gene-targeted loss(es) of function were activated and cultured (1 and 2 d) with αCD40, BAFF, IL-4, and IL-5. Metabolic functions were then assayed by a metabolic flux analyzer. (**b–f**) As for (**a**), except WT cells were treated with inhibitors (CB839; UK5099) alone or in combination, as indicated by the color coding, and then subjected to mitochondrial stress-tested measurements of respiration

Figure 5 continued on next page

Figure 5 continued

(**b**), biochemical assays of [ATP] (**g–i**), flow cytometry (**j, l**), or qPCR (**k**). (**a**) Oxygen consumption rates (OCR) during mitochondrial stress testing of B cells, comparing loss-of-function B cells of the indicated genotypes, color-coded as in ***Figure 3***. (**b–d**) Changes in basal respiration and maximal respiration of B cells from day 1 to day 2 after activation (**b**), calculated from assays in (**c**) and (**d**). OCR values at day 2 were used for statistical analysis. (**c, d**) As in (**a**) except that purified WT B cells were used, with additions of vehicle (DMSO) or the indicated inhibitor(s) (CB839, 1 μM; UK5099, 10 μm), with each B cell pool assayed on both days 1 (**c**) and 2 (**d**) after purification and activation. (**e**) Extra-cellular acidification rates (ECAR) during glycolytic stress tests of WT B cells activated and cultured in the presence of the indicated agents after 2 d cultures as in (**d**). (**f**) ECAR during glycolytic stress test of B cells inducibly rendered $Gls^{\Delta\Delta}$ and/or $Mpc2^{\Delta\Delta}$, then activated and cultured as in (**a**). (**g, h, i**) Intracellular [ATP] in lysates of B cells activated and cultured (2 d) as in (**c**). (**g**) Metabolic inhibitors were present throughout the period of culture (2 d) and assay. (**h**) Cells were activated and initially cultured in the presence of the indicated metabolic inhibitor(s), then washed, and assayed (90 min) in medium without inhibitors. (**i**) After activation and 2 d culture with no inhibitor present, the indicated agent(s) were added to block glutaminolysis and/or mitochondrial pyruvate import during the 90 min assay. (**j**) Mitochondrial membrane potential determined by tetramethylrhodamine (TMRE) staining analyzed by flow cytometry. Shown are mean fluorescence intensity (MFI) values from each independent experiment after activation and culture (2 d) as in (**c**), then normalized to DMSO-treated condition in each experiment. (**k**) Flow cytometry results comparing inhibitor-treated cells vs controls after staining for ROS with DCFDA in three independent replication experiments, with each dot representing one experiment, normalizing as in (**i**).

The online version of this article includes the following source data and figure supplement(s) for figure 5:

Source data 1. Data compendium, experimental results in ***Figure 5*** and ***Figure 5—figure supplement 1***.

Source data 2. Prism file with quantitative data from Seahorse assays of ***Figure 5***.

Source data 3. Additional numerical data on quantitative analyses of metabolic flux analyses (***Figure 5***).

Figure supplement 1. Synthetic auxotrophy of B cell metabolism supports ROS homeostasis and survival in GC B cells.

Figure supplement 1—source data 1. Data of ***Figure 5***, panel j.

Figure supplement 1—source data 2. Data of qPCR results for mitochondrial DNA as in ***Figure 5—figure supplement 1***, panel f.

To evaluate the relationship of STAT3 activity to the metabolic dependence of IL-21-induced proliferation, we then exploited a gain-of-function STAT3 mutant (***Pilati et al., 2011***) in experiments using transduction of B cells that were wild-type or $Gls^{\Delta\Delta}$, $Mpc2^{\Delta\Delta}$ (***Figure 6e and f***). While the division rates of B lymphoblasts deficient in GLS and MPC function were reduced, the subset of $Gls^{\Delta\Delta}$, $Mpc2^{\Delta\Delta}$ B cells transduced with constitutively active STAT3 (i.e. the $Thy1.1^{+}$ cells) exhibited a substantial albeit incomplete restoration of their proliferation (***Figure 6e and f***).

Unexpectedly, computational algorithms identified the IFN-stimulated gene signature as the most prominently impaired pathway in the *Mpc2*, *Gls1* double-deficient GC B cells (***Figure 7a***). Thus, the effects of MPC2 in the setting of GLS depletion were to promote IFN response signatures and Jak-STAT signaling, as well as suites of RNA linked to respiration (***Figure 7b***; ***Figure 4—figure supplement 5a, d***). Among processes that could lead to such a strong effect on mRNA levels, a straightforward possibility was that the metabolism in B cells affects their IFN-elicited signal transduction. Strikingly, IFN-induced phosphorylation of the conserved tyrosine was attenuated when activated cells were treated with CB839 and UK5099 prior to stimulation with type 1 or 2 IFN (IFN-β and -γ, respectively) (***Figure 7c and d***). This effect was observed in B cells 3 days after initial activation via CD40 cross-linking, and inhibition was observed when the pharmacological agents were present only for the final 16 hr, or when anti-CD40-activated blasts were analyzed the day after activation (***Figure 7c and d***). Decreased IFN-stimulated phospho-STAT1 was also observed in comparisons between WT and $Gls^{\Delta\Delta}$ $Mpc2^{\Delta\Delta}$ B cells from tamoxifen-treated mice (***Figure 7—figure supplement 1a–d***). One consequence of STAT1 nuclear translocation and chromatin association is that the C-terminal transcription activation domain (TAD) can become phosphorylated at S727, an event that depends on the Jak/Tyk2 tyrosyl kinase action (***Sadzak et al., 2008***). Of note, IFN-induced STAT1(Y727) phosphorylation also was attenuated when GLS and MPC2 were impeded in activated B cells (***Figure 7c and d***). We conclude that altered intermediary metabolism in B cells can, within less than a day, change IFN receptor induction of phospho-STAT1.

Finally, we tested models of mechanisms that could mediate the observed ability of metabolism (i.e., glutaminolysis and mitochondrial pyruvate import) to increase STAT1 phosphorylation in activated B cells. Flow cytometry results indicated that a simple model in which surface expression of IFN receptors was reduced is unlikely (***Figure 7—figure supplement 1e***), suggesting instead an impairment of receptor signaling to STAT1. One observed effect of the combined metabolic reprogramming was to increase steady-state ROS in both B and GC B cells (***Figure 5k***; ***Figure 5—figure supplement 1a***). Of note, ROS can reduce function of complex I of the electron transport chain (ETC) by modifying

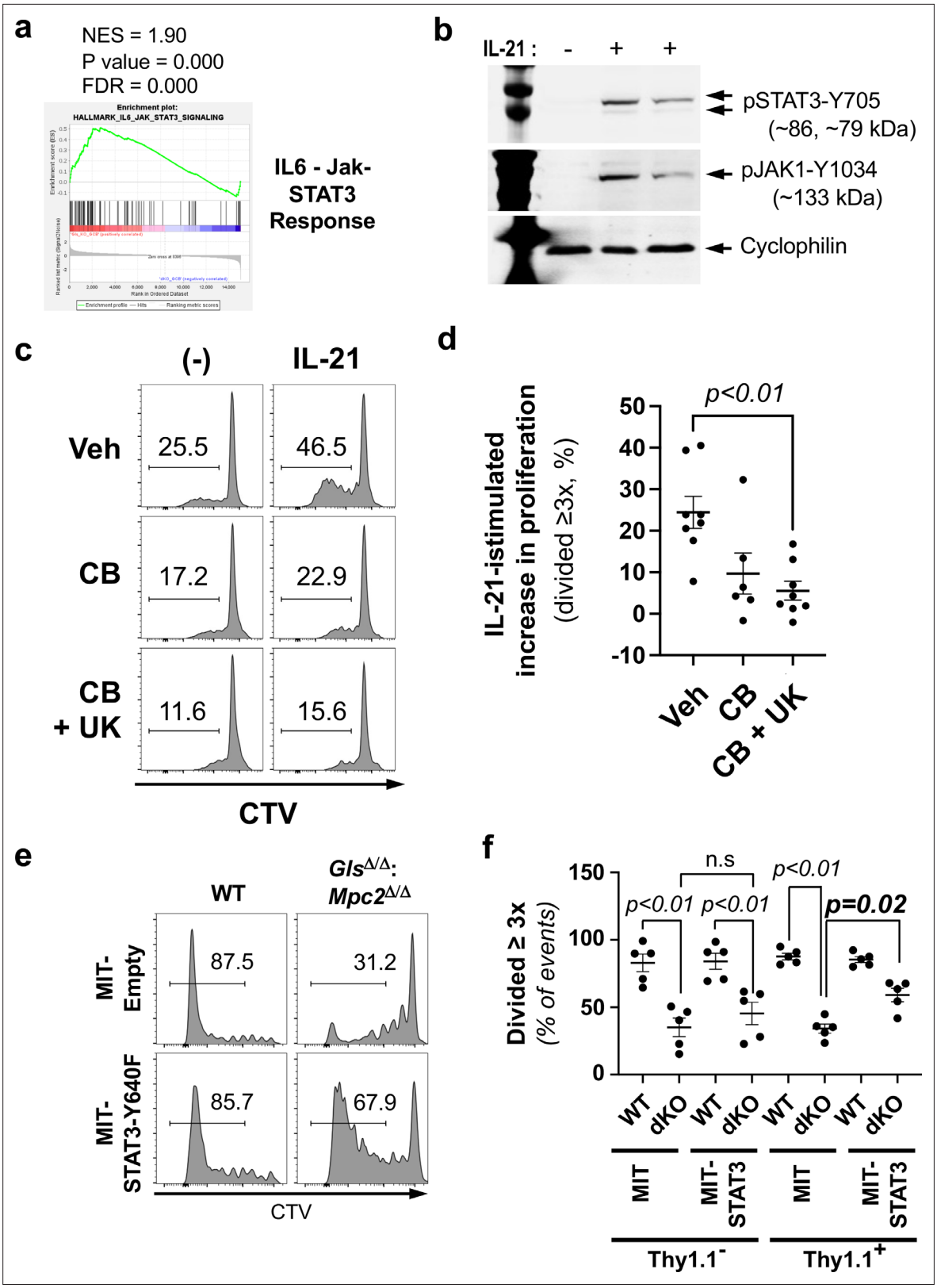


Figure 6. Metabolism in B cells promotes B cell proliferation via IL-21 signaling to STAT3. (**a**) Enrichment of the IL6-stimulated Jak-STAT3-induced gene set. (**b**) Immunoblot analyses of IL-21-induced tyrosine phosphorylation of STAT3 in B cell blasts, showing representative results from one individual experiment representative of three independent replications. Purified B cells were activated with anti-CD40 and BAFF, cultured for 16 hr in the presence of vehicle (DMSO) or inhibitors (CB839 and UK5099), as indicated, then stimulated (15 min) with IL-21. (**c, d**) CB839 and UK4099 attenuate IL-21-

Figure 6 continued on next page

Figure 6 continued

induced B cell proliferation. B cells were stained with CTV, stimulated with anti-CD40 and BAFF with and without CB839 and UK5099 for 3 days in the presence or absence of IL-21. (x=4; n=8). (**c**) Shown are the representative flow plot of CTV partitioning in viable B cell gates. (**d**) Aggregated mean (± SEM) frequencies of IL-21-induced proliferation of B cells calculated by subtracting CTV^{low} frequencies of without IL-21 from with IL-21. p-Values were calculated by Mann-Whitney U test. (**e, f**) Expression of a STAT3 gain-of-function mutant reverses the impact of GLS and MPC2 deficiency on B cell proliferation. WT and $Gls^{\Delta\Delta}Mpc2^{\Delta\Delta}$ (designated here as 'dKO') B cells purified from tamoxifen-injected huCD20-$CreER^{T2}$ mice were transduced with replication-deficient virions of either the MIT retrovector or MIT-STAT3-Y640F (***Pilati et al., 2011***), as indicated, stained with CTV, stimulated with anti-CD40, anti-IgM, BAFF, IL-4, and IL-5, and cultured 5 days. Shown are the flow-cytometry results of a representative analysis of CTV partitioning in Thy1.2-positive transduced cell gates (**e**) and mean (± SEM) frequencies of B cells that divided ≥3 times, aggregating data from three biologically independent replicate experiments (**f**), comprising five separate pools each of WT and $Gls^{\Delta\Delta}Mpc2^{\Delta\Delta}$ ('dKO') samples. p-Values were calculated by Mann-Whitney U test.

The online version of this article includes the following source data and figure supplement(s) for figure 6:

Source data 1. Archive of image and Excel files with source data in support of ***Figure 6***.

Figure supplement 1. Gating to analyze cell division history in B cells transduced with the bi-cistronic MiT retrovector.

reactive sulfhydryl groups in the complex, and elimination of complex I from the mitochondrial ETC decreased IFN-γ activation of STAT1 in a genome-wide loss-of-function screen with an immortalized macrophage-like cell line (***Weisel et al., 2020***). The absence of complex I was mimicked by the ETC inhibitor rotenone (***Kiritsy et al., 2021***). Longer rotenone treatments were highly toxic to B cells, but we found that p-STAT1(Y701) induction in activated B cells was dramatically decreased by a remarkably short (45 min) exposure to this agent prior to IFN stimulation (***Figure 7e and f***). Metformin also inhibits complex I, albeit at higher concentrations than are achieved clinically (***Larsen et al., 2012***; ***Fontaine, 2018***). When tested with activated B cells, this pharmaceutical agent also decreased p-STAT1 elicited by IFN stimulation (***Figure 7e and f***).

Dysfunction or chemical inhibition of ETC complex I causes increased mitochondrial production and export of ROS (***Li et al., 2003***), so it was possible that these results were in part attributable to elevated ROS. Using an approach that had provided evidence of ROS inhibiting STING-dependent IFN-β production (***Tao et al., 2020***), we increased ROS in activated B cells by applying either menadione or H_2O_2 prior to IFN treatment. Menadione substantially reduced induction of P-STAT1 by receptors for both IFN-β and -γ, which was almost completely abrogated by a short-term pre-treatment with H_2O_2 (***Figure 7g and h***). We conclude that increased steady-state ROS and mtROS in B cells, which arise when GLS and MPC function are impaired, contribute to an unexpected defect in IFN-R signaling to STAT1. All together, the results reveal that an interplay between two metabolic pathways progressively reduced the expansion of mitochondrial respiration in B cells. A key functional effect of the combined impairment of two metabolic pathways is the establishment of a block to PC differentiation and high-affinity Ab responses. Unexpectedly, however, the mitochondrial dysfunction and elevated ROS also converged on IFN-receptor signaling and the programming IFN-response functions.

Discussion

We and others have published examples of a metabolic flexibility in B lineage cells that appears to allow limit or negate the effects of loss-of-function mutations in key steps of intermediary metabolism (***Brookens et al., 2024***; ***Bierling et al., 2024***; ***Li et al., 2024***). These findings raise questions as to whether or not there are interventions that could more substantially interfere with the ongoing production of PCs secreting Ab or, conversely, which pathways might need to collaborate for promoting full-strength Ab responses. The work presented here supports three central insights. First, we have identified conditions under which the anti-NP response is relatively glutaminase-independent, both in the primary phase and upon recall stimulation of B cells. Despite this apparent independence, this enzyme central to processing of glutamine and to anaplerosis takes on a vital role if mitochondrial pyruvate import is impeded. A related point is that the findings underscore the fallacy in stating conclusions as if universally applicable, inasmuch as the effect of B cell specific loss-of-function for GLS depended on the nature of the immunization. Thus, the anti-ovalbumin response derived from GLS-depleted B cells was substantially reduced under one set of conditions where the anti-NP responses after multivalent hapten-carrier immunization with NP were not similarly reduced after isolated *Gls* gene inactivation. Mechanistically, the findings revealed that glutaminase activity promotes a

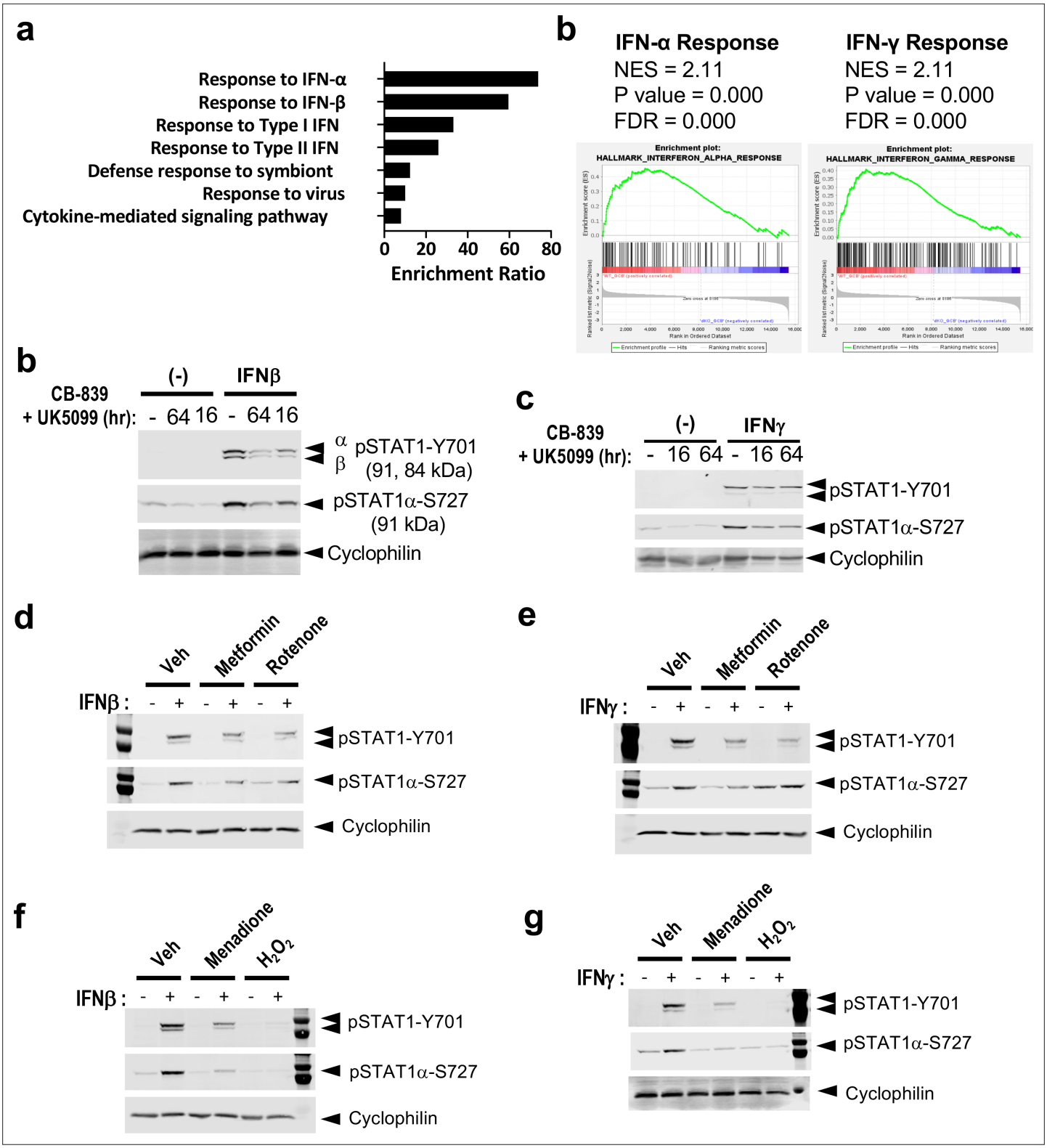


Figure 7. Metabolic programming in B cells modulates interferon signaling to STAT1. (**a**) Results from an over-representation analysis of differentially expressed protein-coding RNA in WT versus induced double-deficient (*Gls*$^{\Delta\Delta}$*Mpc2*$^{\Delta\Delta}$) B cells, as counted in the RNA-seq analyses with GC B cells of SRBC-immunized mice (as in ***Figure 4***, (**j–l**)). Additional GSEA and an overview of gene set comparisons for pairs of genotypes are presented in ***Figure 4—figure supplement 5***. (**b**) Selected analyses of gene sets enriched in WT GCBs compared to their counterparts subjected to disruption of both *Gls* and *Mpc2* (*Gls*$^{\Delta\Delta}$*Mpc2*$^{\Delta\Delta}$ GCBs) using the Hallmark Pathway database. Shown are enrichment of IFN-α- and IFN-γ-associated pathways in

Figure 7 continued on next page

Figure 7 continued

WT GCBs compared to the *Gls*$^{\Delta\Delta}$, *Mpc2*$^{\Delta\Delta}$ samples. (**c–h**) Immunoblot analyses of IFN-induced STAT1 phosphorylation in activated B cells, showing representative results from individual experiments, each representative of three independent replications. (**c, d**) Purified B cells were activated with anti-CD40 and BAFF and cultured for 64 or 16 hr in the presence of vehicle (DMSO) or inhibitors (CB839 and UK5099), as indicated, then stimulated (15 min) with IFN-β (**c**) or IFN-γ (**d**) followed by immunoblotting using Ab specific for p-STAT1(Y701) or p-STAT1α(S727) along with anti-cyclophilin B Ab as a loading control. (**e, f**) Inhibition of mitochondrial ETC attenuates STAT1 activation. B cells were activated and cultured as in e and f but for 16 hr, in the presence or absence of metformin (2 mM; 16 hr) or rotenone (0.5 μM; final 2 hr of the cultures) as indicated, then stimulated (15 min) with IFN-β (**g**) or IFN-γ (**h**) and analyzed as for panels c and d. (**g, h**) ROS inhibit STAT1 activation. B cells were activated and cultured for 16 hr, in the presence or absence of menadione (2 μM; all 16 hr) or H_2O_2 (100 μM; the final 2 hr), and then stimulated with IFN-β (**g**) or IFN-γ (**h**) for 15 min.

The online version of this article includes the following source data and figure supplement(s) for figure 7:

Source data 1. Archive of image and Excel files with source data in support of ***Figure 7***.

Figure supplement 1. Normal IFN-R expression yet decreased P-STAT1 in metabolically reprogrammed B cells.

Figure supplement 1—source data 1. Archive of image and Excel files with source data in support of ***Figure 7—figure supplement 1***.

progressive increase in mitochondrial respiration in a manner enhanced by pyruvate import, an alternative pathway for providing substrates to the TCA (Krebs) Cycle. A third major finding is that the efficiency of coupling IFN receptors to the tyrosyl and serine phosphorylation of STAT1 – and IL-21 stimulation to STAT3 – depends on the programming of intermediary metabolism in a manner linked to ROS homeostasis. Taken all together, the findings reveal not only new insights into how intermediary metabolism can modulate differentiation and receptor signaling, but suggest the potential for new interventions in autoimmune diseases driven by IFN effects and auto-Ab.

Although the impetus to this work is a basic question about the interplay of intermediary pathways of intracellular metabolism, a major practical implication of the findings presented here is translational. A self-reinforcing network of increased IFN production and pathological levels and persistence of auto-Ab production is characteristic of several autoimmune conditions of humans. SLE and rheumatoid arthritis (RA) are most common and studied, but this pairing also is involved in inflammatory myopathies and primary Sjogren's syndrome (***Rönnblom and Eloranta, 2013***; ***Higgs et al., 2011***). Effectiveness of therapeutic mAb for B cell depletion is best established in RA; unimpressive results in SLE raised concerns that disease might be perpetuated by long-lived PC that secrete auto-Ab, do not need BAFF, and are CD20^{neg}. However, dramatic results of testing CD19-directed chimeric Ag receptor T cells in patients with SLE and myositis showed that targeting B cells reduced clinical disease, IFN levels, and those of pathologic auto-Ab [(***Müller et al., 2024***), reviewed in ***Taubmann et al., 2024***]. These effects imply that ongoing production of PC from B cells maintains IFN production and disease activity. Cost, production complexity, and risk profile mean that a need to identify other approaches that restrict the ongoing differentiation of B cells into PC remains, despite the dramatic results in patients with severe disease. The capacity of CB839 to collaborate with UK5099 to suppress both PC differentiation and responsiveness to IFNs suggests that this agent and glutaminase-specific inhibition in general merit further analysis. Since CB839 appeared safe in patients during phase 2 clinical testing (***Lee et al., 2022***), our finding of an interplay between the standard-of-care agent HCQ and CB839 in the inhibition of PC development in vitro similarly militates in favor of translational investigation. Which B cells are major sources of the PC that secrete pathological auto-Ab, and the extent to which SLE susceptibility might involve a distinct relationship between intermediary metabolism and PC differentiation, are important issues beyond the scope of the present study. Although the atypical MBC that are implicated in SLE pathogenesis (***Dörner and Lipsky, 2024***) were not specifically tested and one cannot exclude some contribution of Ag being presented to the remnant GC that persisted after primary immune challenge, our data suggest that inhibition of the pathways impacted MBCs that rapidly differentiated after a secondary challenge.

Another finding of the work bears both on consideration of the intersection of B cell metabolism and function after immunization, and perhaps on the relationship of our findings to SLE. Our data show that although the Ag-specific Ab response elicited by a protein, ovalbumin, was reduced by B cell-specific depletion of GLS in an allergic lung inflammation model of immunization, the anti-NP response was normal. Our finding that the metabolic requirements for Ab responses differed according to Ag or type of immunization raises questions that merit being worked out in future research. A key point is that immunization to elicit anti-NP responses usually is carried out with heavily haptenated carriers, that is many NP-groups on each protein molecule. In sharp contrast, a particular epitope in

the carrier protein (ovalbumin, KLH, gamma globulin) will be monovalent unless part of an aggregate. Valency and the extent of BCR cross-linking influence signaling by the BCR, which in turn can affect metabolic regulators such as mTORC1 and c-Myc. A related possibility derives from the characteristics of the anti-NP response, which is dominated by a limited Ig heavy chain repertoire (***Cumano and Rajewsky, 1985***). Thus, intrinsic biochemical characteristics of V_H125:$V_L\lambda$ BCR interactions with NP might lead to programming metabolic requirements that differ from what is elicited by the BCR repertoire responding to ovalbumin. The issue of valency has a bearing on the pathological Ab in auto-immunity in that so many auto-Ab of SLE are directed against multivalent Ag such as dsDNA and ribonucleoprotein complexes (***Olsen and Karp, 2014***; ***Suurmond and Diamond, 2015***; ***Tsokos et al., 2016***; ***Caielli et al., 2023***). Finally, the specific immunization regimen might affect the results. General issues of valency in engagement of BCR at the cell surface remain incompletely clarified despite years of papers, so extensive further studies will be needed to understand better the relationship to a specific step in intermediary metabolism. Nonetheless, a striking finding herein is that a vital requirement for glutaminolysis is cryptic in the anti-NP response until uncovered by reduced import rates of either glucose into cells or pyruvate into mitochondria.

Our findings directly connect to questions of metabolic flexibility, which is a central issue for the potential translatability or implications of intermediary metabolism in targeting immune responses or auto-immunity. Targeting a particular process is less likely to be efficacious to the extent that GC B cells, or B cells in general, can use alternatives and achieve normal responses or outputs. For instance, although there is evidence that the majority of energy generation by activated and GC B cells involves FA oxidation, most of it in mitochondria (***Weisel et al., 2020***; ***Li et al., 2024***), elimination of a key step in mitochondrial acquisition and use of FAs had no impact on Ab responses or discernible reduction in GC or affinity maturation (***Li et al., 2024***). Alternatively, restricting cell-intrinsic generation of serine from a glycolytic intermediate represents one potential point of vulnerability that was not compensated by flexibility (***D'Avola et al., 2022***). Depletion of a major glucose transporter – and inferentially of reduced supply of glucose for some combination of NADPH regeneration from NADP, serine biosynthesis, oxidation, and perhaps other uses of glucose – also reduced GC size, Ab responses, and affinity maturation (***Brookens et al., 2024***; ***Bierling et al., 2024***). However, the effect magnitude (reduction to ~1/4 normal) appeared less promising from the standpoint of potential treatment of autoimmunity. Metabolomic data suggested that increased anaplerosis was a compensatory mechanism that might have limited the severity of the defect in ASC generation and Ab responses of GLUT1-depleted B cells (***Bierling et al., 2024***). Our findings support this inference in that the defects with *Slc2a1*$^{\Delta\Delta}$ or *Mpc2*$^{\Delta\Delta}$ B cells were each dramatically amplified by impedance of glutaminolysis. The size of the differences, the impact on the IgG2(a/)c isotype that is particularly important in SLE pathogenesis (reviewed in ***Bonanni et al., 2015***), and the vital functions of STAT1 induction by IFN receptors in autoimmune models (***Domeier et al., 2016***; ***Domeier et al., 2018***) indicate that this synthetic auxotrophy merits translational consideration. Inasmuch as cancer cells commonly have increased ROS levels at steady state (***Akter et al., 2026***).

The finding that metabolism regulates cytokine receptor coupling to Jak-STAT pathways raised a subsidiary question. Might there be conditions in health or disease, independent from genetic or pharmaceutical loss of function, where reduced rates of αKG production co-exist with decreased glucose import or pyruvate import into mitochondria? Some tumor masses had low interstitial glucose (***Ho et al., 2015***; ***Chang et al., 2015***), and insufficient dietary protein intake causes a substantial reduction in circulating glutamine (***Nohr et al., 1986***; ***Andrews and Griffiths, 2002***; ***Taylor et al., 2013***; Raybuck and Boothby, unpublished data). Thus, decreased glutamine and glucose utilization may co-exist during short-term protein malnutrition after surgery of patients with residual tumor masses. A related circumstance could be for B cells in hypoxic regions of a tumor mass in cancer. Hypoxia tends to activate pyruvate dehydrogenase kinases, enzymes that decrease the generation of Ac-CoA from pyruvate, and indeed may also decrease mitochondrial pyruvate import (***Golias et al., 2016***; ***Ruiz-Iglesias and Mañes, 2021***). Although hypoxia tends to increase glutamine uptake in cancer cell models, our prior work indicated that this stimulus and HIF stabilization in B cells decreased their uptake of a.a. such as glutamine. Moreover, decreased glutaminolysis by cancer cells (i.e. their glutamine use) increased micro-environmental glutamine and the functionality of tumor-infiltrating lymphocytes – indicating that glutamine was limiting in the TME (***Edwards et al., 2021***) – as has been reported for glucose (***Ho et al., 2015***; ***Chang et al., 2015***). Since IFN-γ responsiveness is crucial in

anti-tumor immunity and B cells tend to contribute to checking tumor growth (reviewed in ***Ikeda et al., 2002***; ***Sarvaria et al., 2017***; ***Laumont et al., 2022***), the findings here have potential implications for one means by which cancer cell effects on nutrient micro-environments may assist in immune evasion.

Materials and methods

Mice and immunizations

All animal protocols – reviewed and approved by Vanderbilt University Institutional Animal Care and Use Committee – complied with the National Institutes of Health guidelines for the Care and Use of Experimental Animals. Mice were housed in specified pathogen-free conditions. Both male and female mice, aged 6–10 weeks, were used; sex-specific subgroup analyses did not reveal any significant differences and yielded the same conclusions. To enable tamoxifen-induced, B cell type-specific inactivation of GLS, GLUT1, and/or MPC2 coding potential, *Gls*$^{f/f}$ (***Johnson et al., 2018***) *Slc2a1*$^{f/f}$ (***Caro-Maldonado et al., 2014***), and *Mpc2*$^{f/f}$ mice (***Lam et al., 2016***) were crossed with *huCD20*-CreER^{T2} (***Khalil et al., 2012***) transgenic mice; for confirmatory in vitro work with purified B cells, some experiments used *Rosa26*-CreER^{T2} (as in ***Cho et al., 2016***). Tamoxifen was administered as reported previously (***Cho et al., 2016***; ***Brookens et al., 2024***). To control for potential Cre toxicity in B cell responses or GC B cells, age-matched *Gls*$^{+/+}$, *Slc2a1*$^{+/+}$, and *Mpc2*$^{+/+}$, *huCD20*-CreER^{T2} mice were co-housed with *huCD20*-CreER^{T2} mice that had conditional alleles [*Gls*$^{f/f}$, *Slc2a1*$^{f/f}$, and/or *Mpc2*$^{f/f}$], alone or in combination, and used as wild-type controls.

Mice were immunized, or immunized and boosted, by one or two intraperitoneal (i.p.) injections of 100 µg of 4-hydroxy-3-nitrophenylacetyl hapten (NP) conjugated to ovalbumin (NP-ova, Biosearch Technologies, Novato, CA), emulsified in 100 µL alum Imject alum (Thermo Fisher Scientific, Pittsburgh, PA), as described previously (***Cho et al., 2016***; ***Brookens et al., 2024***; ***Raybuck et al., 2018***), or after this product was discontinued, Alhydrogel 2% (InvivoGen, San Diego, CA). For mucosal challenges to elicit an anti-carrier Ab response, ovalbumin (50 µg dissolved in 20 µL PBS) was instilled intranasally (i.n.) once daily across seven consecutive days starting 3 weeks after i.p. initial sensitization of mice with NP-ova. Mice were harvested 12 h after the final inhalation. Alternatively, mice were immunized with sheep red blood cells (SRBC) as described (***Cho et al., 2016***), and harvested at seven days after immunization. Harvested spleens in some experiments were used to purify GC B cells for RNA-seq (detailed below) after tamoxifen injections and SRBC immunization (***Figure 4j–l***). To assess proliferation rates of GC B cells in vivo, intravital BrdU incorporation measured by injecting mice with 2 mg BrdU (Sigma-Aldrich, St. Louis, MO) 16 hr and 4 hr before harvesting spleens from SRBC-immunized mice. Single-cell suspensions, prepared as described above, were stained for surface markers (B220, IgD, GL7, CD38; dump channel markers as specified in the Flow Cytometry section) followed by cell fixation, permeabilization, and staining BrdU-containing DNA using the APC BrdU Flow Kit (B-D Pharmingen, San Jose, CA) according to the manufacturer's protocol. GC B cells were defined as B220^{+} GL7^{+} IgD^{neg} CD38^{neg}, as control analyses have shown that a CD138^{+} pre-PC population is <2% of this gate.

Flow cytometry

Fluor-conjugated mAbs were purchased from BD Pharmingen (San Jose, CA), Life Technologies, eBiosciences (San Diego, CA), or Tonbo Biosciences. For detection of GC- and memory-phenotype B cells in the spleens of immunized mice, samples were stained as previously described (***Paus et al., 2006***). In brief, 3x10^{6} splenocytes were stained with anti-B220, -GL7, -Fas, -IgD, -CD38, NP-APC, and a dump channel containing anti-CD11b, -CD11c, -F4/80, -Gr-1, and viability marker (7-AAD or Ghost-Brilliant Violet 510) in 1% BSA and 0.05% sodium azide in PBS. For detection of PC in products of in vitro cultures, viable cells (gated via FSC, SSC, and Ghost e450) were stained with fluorophore-conjugated anti-CD138, -B220, -CD19, or -TACI. For flow analyses of mitochondrial and total intracellular ROS, cells (1–3 × 10^{6}) were washed in PBS and stained with 40 nM MitoTracker Green, 10 nM TMRE, 5 µM MitoSOX, or 1.25 µM H_2DCFDA, respectively, along with Ghost-780 in PBS (20 min at 37 °C), then washed again (1% BSA in PBS) and further stained with anti-B220, -CD19, -CD138, or -TACI. Samples were analyzed using a FACS Canto flow cytometer driven by BD FACS Diva software or as part of

preparative flow purification with a FACS Aria flow sorter. Data were processed using Flow-Jo software (FlowJo LLC, Ashland, OR).

Cell cultures and reagents

B cells were purified from mouse spleens using negative selection with biotinylated anti-CD90 and an iMag system (BD-Pharmingen) or positive selection with anti-mouse B220 nanobeads (Miltenyi Biotec, Auburn CA). To induce PC differentiation, B cells (seeded at 5×10^5/mL) were cultured with 1 µg/mL anti-CD40 (Tonbo, San Diego CA), 10 ng/mL BAFF (AdipoGen, San Diego, CA), 10 ng/mL IL-4 (Peprotech, Rocky Hill, NJ), 5 ng/mL IL-5 (Peprotech), and, if derived from inducible gene deletion models, 50 nM 4-hydroxy-tamoxifen (4-OHT) (Sigma-Aldrich, St. Louis MO) and re-fed at day 3. When cultured 2 d or less, cells were in the same conditions after plating at 2×10^6/mL. Alternatively, B cells were cultured and analyzed as for anti-CD40-activated cells after activation with both Fab_2' anti-mouse IgM (Southern Biotech, Birmingham, AL; 1 µg/mL) and anti-CD40 (1 µg/mL). Glutamine supplementation analyses, with or without added DMK (5 mM), were performed using glutamine-free RPMI (Thermo Fisher, Waltham MA) supplemented with 10% dialyzed Gibco FBS (Thermo Fisher), 100 U/mL penicillin (Invitrogen, Waltham MA), 100 µg/mL streptomycin (Invitrogen), non-essential amino acids (NEAA, Invitrogen), with or without 10 mM HEPES (Invitrogen), and 0.1 mM 2-mercaptoethanol (Sigma). To test how inhibitors affected in vitro proliferation, cytokine receptor signaling, or PC differentiation, cultures were supplemented with 1 µM CB839, 10 µM UK5099, and/or 3 µM HCQ (all from Cayman Chemical Co, Ann Arbor MI), individually or in combinations, and 1 mM DMK was used to supplement some cultures subjected to glutaminolysis inhibition by CB839. To analyze proliferation in vitro, B cells (2×10^6, purified as above) were labeled with 5 µM CellTrace Violet (CTV; Invitrogen, Waltham, MA) and then activated and cultured as above. To test the impact of ROS and ETC inhibition on activation of STAT transcription factors, cultures of B cells activated with anti-CD40, BAFF, IL-4, and IL-5 were supplemented with 0.2 mM H_20_2 (Sigma-Aldrich), 2 µM menadione (Sigma-Aldrich), 2 mM metformin (Sigma-Aldrich), or 1 µM rotenone (Calbiochem, San Diego CA).

Retroviral transduction

Plasmids encoding the bicistronic retrovector MIT (***Mitchell et al., 2001***) or a construct encoding STAT3-Y640F (***Pilati et al., 2011***) inserted into MIT were transfected into ΦNX ecotropic packaging cells, whose supernatant media were then used for 'spinfection' of B cells as described (***Cho et al., 2016***). For retroviral transduction to test the reversion of GLS1 and MPC2 deficiency on B cell proliferation and differentiation, splenic B cells from tamoxifen-treated huCD20-CreER^{T2+} ("WT") or *Gls1*$^{f/f}$; *Mpc2*$^{f/f}$; huCD20-CreER^{T2+} mice were purified by Thy1.2 depletion and transduced with retrovirus MIT or the gain-of-function mutant MIT-STAT3-Y640F (***Pilati et al., 2011***). The B cell pools were then stained with 5 µM CTV, activated, and cultured in the presence or absence of IL-21 as above, and analyzed by flow cytometry.

ELISA and ELIspot

Relative NP-specific Ab concentrations in sera, and secreted Ab in culture supernatants, were measured using capture ELISA as described previously (***Cho et al., 2016***; ***Brookens et al., 2024***; ***Raybuck et al., 2018***). All- or high-affinity hapten-specific Ab were measured using plates coated with NP_{20}-BSA or NP_2-PSA (Biosearch Technologies), respectively. Ovalbumin-specific antibodies were measured using serial dilutions of sera incubated on ovalbumin (1 µg/well)-coated 96-well plates (16 hr at 4 ° C). Total secreted Ab were captured using an anti-Ig(H+L) reagent. Captured Ab retained after rinsing were detected in an isotype-specific manner using HRP-conjugated anti-IgM, -IgG1, IgG2c, or -IgE incubation and colorimetric development with Ultra TMB Substrate (Thermo Fisher Scientific).

The frequencies of antibody secreting cells (ASCs) in the bone marrow, lung, or spleen after immunization were measured as described previously (***Brookens et al., 2024***; ***Raybuck et al., 2018***). Briefly, high protein binding plates (Corning Life Science, Corning NY) were coated with NP_{20}-BSA (for all-affinity ASCs) or NP_2-PSA (for high-affinity ASCs; Biosearch Technologies), then seeded with splenocyte suspensions ($0.5–1\times10^6$ cells/well [IgM], $1–2\times10^6$ cells/well [IgG1], and 2×10^6 cells/well [IgG2c]), cultured in medium with 10% FBS (16 hr), and probed with biotinylated anti-IgM, anti-IgG1, or anti-IgG2c antibodies (Southern Biotechnologies, Birmingham AL). For the detection of IgM or IgG1 ASC in day 5 in vitro cultures, high protein binding plates were coated with anti-Ig(H+L) (Southern

Biotechnologies), seeded with suspensions of cultured cells (20 hr, with 100, 200, and 500 cells per well [IgM] or 1000, 2000, and 5000 cells/well [IgG1]), then probed with biotinylated anti-IgM or -IgG1 antibodies (Southern Biotechnologies, Birmingham AL). ASC numbers and spot sizes were quantified using an ImmunoSpot Analyzer (Cellular Technology, Shaker Heights, OH) and the densities based on dilutions with readily resolved spots.

Nucleic acid analyses

RNA was isolated from sorted B cells or in vitro-generated B lymphoblasts using TRIzol reagent following the manufacturer's instructions (Life Technologies, Carlsbad, CA). RNA from cultured B cells purified from TriZol and processed for bulk RNA-seq by the VANTAGE Core of the Vanderbilts. To assess the extent of the loss-of-function in B cell populations, gene expression was analyzed using quantitative real-time RT-PCR (qRT^2-PCR). After cDNA synthesis by reverse transcription with an AMV Reverse Transcriptase kit (Promega, Madison, WI), amplifications were performed using SYBR Green Power UP PCR master-mix (ThermoFisher Scientific) and primer pairs specific for *Gls* (Forward 5′-GGGAATTCACTTTTGTCACGA-3′; Reverse 5′-GACTTCACCC TTTGATCACC-3′), *Mpc2* (Forward 5′-TGTTGCTGCCAAAGAAATTG-3′; Reverse 5′-AGTGGACTGAGCTGTGCTGA-3′), and β-actin (Forward 5′-GGCACCACAC CTTCTACAATG-3′; Reverse 5′-GGGGTGTTGAAGGTCTCAAAC-3′). The relative level of gene expression was calculated using the 2-DDCT method after each sample was normalized to β-actin. Libraries for low-input bulk RNA-seq analyses with flow-purified GC B cells were generated and sequenced essentially as described (***Scharer et al., 2020***) and sequenced at the Emory Integrated Genomics Core. In brief, for each sample, 1000 cells were sorted directly into RLT buffer (79216; Qiagen) containing 1% (v/v) 2-mercaptoethanol. RNA was isolated using Zymo Quick-RNA MicroPrep Kit (11–328 M; Zymo Research). Synthesis of cDNA was performed using SMART-Seq v4 Ultra Low Input RNA Kit (634894; Takara Bio) kit. Final libraries were generated using 200 pg of cDNA as input for the NexteraXT kit (Illumina, FC-131–1024) with 12 cycles of PCR amplification. Final RNA-seq libraries were quantitated by QuBit (Life Technologies, Q33231), size distributions determined by bioanalyzer (Agilent 2100), pooled at equimolar ratios, and sequenced at the Emory Genomics Core on a NovaSeq6000 using a PE100 run. The RNA-seq samples of a biologically independent replication set of flow-purified GC B cells from immunized mice representing the four different genotypes were sequenced at Novogene on a NovaSeq X Plus using a PE150 runBulk RNA-seq. RNA from cultured B cells was performed by similar methods at the Vanderbilts' VANTAGE core.

To analyze sequencer outputs of each core, Fastq files were assessed for quality using FastQC. Adapters were trimmed using TrimGalore, followed by FastQC to validate adapter removal. hisat2 was used to align fastq files to the mm10 genome downloaded from UCSC genome browser. Qualimap was used to analyze the aligned sequences for quality. Subread's featureCounts was used to count and normalize sequence counts in groups being compared. featureCount outputs were then used for DESeq2 analysis to identify fold change and significance of observed differences in gene expression. Normalized RNA-Seq counts were analyzed using GSEA 4.3.2 (Broad Institute) and the Hallmark gene sets collection from the Molecular Signatures Database (MSigDB) to identify changes in biological pathways. Differentially expressed genes identified by DESeq2 were analyzed using the MyGeneset tool from the Immunological Genome Project (Immgen) to identify B cell subsets associated with genes affected by intervention in metabolic pathways. The web-based gene set analysis toolkit (WebGestalt) was used for gene ontology over-representation analysis of biological processes using the protein coding genome as the reference set. Differentially expressed genes identified by DESeq2 were analyzed with WebGestalt to identify biological processes implicated by the change in gene expression.

Metabolic analyses

For proton nuclear magnetic resonance spectroscopy (^{1}H-NMRS) quantitation of metabolites in solution, plasma and lymph node interstitial fluids were collected and processed as previously reported (***Haslene-Hox et al., 2011***; ***Edwards et al., 2021***). In brief, a total of 50 µL deuterated water (D_2O) and 50 µL of 0.75% sodium 3-trimethylsilyl-2,2,3,3-tetradeuteropropionate (TSP) in D_2O were added to 500 µL of diluted biological fluids and transferred to 5 mm NMR tubes (Wilmad- LabGlass, Kingsport, TN). ^{1}H-NMRS spectra were acquired on an Avance III 600 MHz spectrometer equipped with a Triple Resonance CryoProbe (TCI) (Bruker) at 298 K with 7500 Hz spectral width, 32,768 time domain

points, 32 scans, and a relaxation delay of 2.7 s. The water resonance was suppressed by a gated irradiation centered on the water frequency. The spectra were phased, baseline corrected, and referenced to TSP using Chenomx NMR Suite. Spectral assignments were based on literature values.

Oxygen consumption rate (OCR) and ECAR were measured using a Seahorse Bioscience XFe96 extracellular flux analyzer (Agilent Technologies, Santa Clara CA). B cells ($2.5x10^5$) activated for 2 days with anti-CD40, BAFF, IL-4, and IL-5 were seeded per well of a Cell-Tak (5 µg/mL; Corning) coated plate. Glycolytic and mitochondrial stress tests were performed as previously described (***Brookens et al., 2024***; ***Raybuck et al., 2018***). Basal respiration, maximum respiration, and ATP production were calculated using formulas derived from the software accompanying the Agilent Seahorse platform. Steady-state ATP concentrations in activated B cells were measured using the Promega Mitochondrial ToxGlo Assay (Promega, Madison WI), following the manufacturer's protocol. B cells activated and cultured 2 d in anti-CD40, BAFF, IL-4, and IL-5 after negative selection of splenocytes with anti-Thy1.2, in the presence or absence of metabolic inhibitors (CB839, UK5099, or both). Equal numbers of viable (Trypan $Blue^{neg}$), washed twice with warm, sterile PBS, were resuspended in glucose-supplemented RPMI1640, with their designated drug treatment added, and cultured (10^5 B cells in 100 µL) 90 min at 37 °C. Cytotoxicity Reagent (20 µL 5 x) was added to each well followed (30 min) by quantifying fluorescence (520–520 nm Em; 485 nm Ex/). 100 µL of ATP Detection Reagent was then added to each well followed by orbital shaking (500 rpm for 5 min). Luminescence was then measured to quantify ATP present in the B cells.

For metabolomic analyses, frozen (–70 C) cell pellets were extracted in plastic vials with 40 µL of UPLC grade isopropanol, sonicated (3 cycles, 10 seconds each), and clarified by centrifugation (20 min). Total protein content was measured using Pierce BCA Protein Assay kit (Thermo Fisher Scientific). Supernatants were analyzed using the Biocrates MxP Quant 500 XL targeted metabolomic kit (Biocrates Life Sciences AG, Innsbruck, Austria), potentially quantitating 106 small molecules and free FAs in chromatography mode and 913 complex lipids in flow-injection mode (FIA-MS/MS).

Metabolite identification was based on triple quadrupole ultra-high-performance liquid chromatography tandem mass spectrometry (UHPLC-MS/MS) using a Shimadzu Nexera chromatography platform (Shimadzu Corporation, Kyoto, Japan) coupled to Sciex QTRAP 7500 mass spectrometer (AB Sciex LLC, Framingham, Massachusetts, USA). Metabolic indicators (474) were then calculated from sums or ratios of relevant metabolites according to Biocrates MetaboINDICATOR formulas (***Limonciel, 2020***). These indicators can be regarded as physiologically relevant measures and are statistically analyzed separately from metabolites. In addition, indicators denoted as 'X synthesis' were computed as a ratio of metabolite X and its main precursors as a reflection of the inferred conversion ratio. Using solvents of LC/UHPLC-MS grade, cleared extracts were transferred onto a kit plate with pre-injected internal standards, dried, derivatized with 5% phenylisothiocyanate in pyridine, ethanol, and water (1:1:1 v/v/v), and subsequent extraction with 5 mM ammonium acetate in methanol. UHPLC was performed with 0.2% formic acid in acetonitrile (organic mobile phase) and 0.2% formic acid in water (inorganic mobile phase). Flow-injection analysis was performed with methanol and Biocrates MxP Quant 500 XL additive. Sample handling, randomized with stratification prior to processing to avoid potential biases, was done on dry ice to avoid multiple freeze-thaw cycles. Plates included isopropanol blanks to calculate limits of detection, repeats of a kit quality control sample to calculate concentrations and monitor the coefficient of variation, and kit calibrators for seven-point calibrations of certain compounds. Analytes (metabolic indicators) were calculated according to Biocrates MetaboINDICATOR formulas (***Limonciel, 2020***). Ratios with zeros in the denominator were treated as missing values that were not considered in the analysis. As additional data transformations, Box-Cox transformation with R package *car* (***Fox and Weisberg, 2018***), and Tukey's fencing (***Tukey, 1977***) were applied for metabolomic data. Furthermore, the values were standardized with respect to the DMSO group to facilitate comparison of regression coefficients in the statistical analysis.

Measurement of cytokine-induced STAT phosphorylation

To measure the levels of total and phosphorylated proteins, B cells were stimulated with anti-CD40 and BAFF, cultured in the presence or absence of inhibitors as detailed in ***Figure 6*** and its Legend, and stimulated (25 min) with IFNβ, IFNγ, or IL-21. Total cell lysates were prepared with modified RIPA lysis buffer (50 mM Tris·Cl (pH 8.0), 150 mM NaCl, 1% NP-40, 0.1% SDS, 1 mM EGTA, 1 mM Na_2VO_4, 1 mM NaF, and protease inhibitor cocktail). Proteins resolved by SDS-PAGE were transferred onto

Immobilon Nylon membranes (Millipore) that were then incubated with anti-phospho-STAT1-Y701 Ab, anti-phospho-STAT1-S727 Ab, anti-phospho-STAT3-Y705 Ab, anti-GLS1 Ab, or anti-cyclophilin Ab followed by fluorophore-conjugated, species-specific secondary anti-Ig Abs (Rockland Immunochemicals and LI-COR). Proteins were visualized and quantitated by Odyssey infrared imaging scanner (LI-COR).

Statistical analyses

Data are reported based on results replicated in at least three biologically independent performances. The primary analyses were conducted on pooled data points from independent samples and replicate experiments, *t* testing with post-test validation of its suitability. Tests used in particular settings are generally indicated in the Figure Legends. In experiments with individual analyses and comparisons of limited numbers of samples, t-tests or non-parametric formulae were applied as appropriate, based on modeling of the similarity of variances between data from the two conditions being compared, and of the estimated fit to Gaussian distributions; Mann-Whitney testing was used if statistical analysis indicated that the two sample sets probably had unequal variance. Data are displayed as mean (± SEM); conventionally, a difference is considered 'statistically significant' when the p value for the null hypothesis of a comparison was <0.05. In addition to the application of this method to individual features in the metabolomic analyses, a series of multivariable linear regression models were employed, each corresponding to a specific analyte, to analyze differences in metabolomic data. In these models, the values of the analytes served as the dependent variables, while individual non-DMSO treatment groups were included as key independent variables, that is considering the DMSO group as the reference.

Acknowledgements

Experimental work was supported by NIH grant R01 AI113292 followed by AI149722 (MRB). and Pathology-Microbiology-Immunology (PM&I) departmental funds. SK Brookens was supported by a supplement to AI113292. We thank D Bhattacharya (U of AZ) for generously shipping *Mpc2* f/f breeding stock essential for this work, X Ye for helpful advice in RNA-seq analyses, MA Jones (Biocrates, Inc) for facilitating the metabolomic analysis, the Emory Integrated Genomics Core Facility (RRID:SCR_023529) for added support of the efforts, and Vanderbilt institutional cores (High-Throughput Screening; Flow Cytometry Shared Resource; Small Molecule NMR; Cell Imaging Shared Resource; VANTAGE) for equipment, expertise, and assistance. NIH Institutional Equipment (S10) grant 1S10OD018015 was instrumental in the acquisition of equipment for metabolic flux analyses and flow cytometry, and scholarships via the Cancer Center Support Grant (CA068485) and Diabetes Research Center (DK0205930) helped defray costs of Vanderbilt Cores.

Additional information

Competing interests

Jeffrey C Rathmell: Was once involved with Citryx (see manuscript). The other authors declare that no competing interests exist.

Funding

Funder	Grant reference number	Author
National Institutes of Health	AI1149722	Shawna K Brookens Ariel L Raybuck Kaylor Meyer Yeeun Paik Mark R Boothby

Funder	Grant reference number	Author
National Institutes of Health	AA113292	Shawna K Brookens Ariel L Raybuck Jennie Hamilton Jingxin Li Juyeon Lim Mark R Boothby

The funders had no role in study design, data collection and interpretation, or the decision to submit the work for publication.

Author contributions

Sung Hoon Cho, Conceptualization, Data curation, Formal analysis, Supervision, Investigation, Visualization, Methodology, Writing – original draft, Project administration, Writing – review and editing; Shawna K Brookens, Conceptualization, Data curation, Formal analysis, Investigation, Writing – review and editing; Ariel L Raybuck, Conceptualization, Formal analysis, Supervision, Funding acquisition, Validation, Investigation, Visualization, Project administration; Kaylor Meyer, Data curation, Formal analysis, Validation, Investigation, Methodology, Writing – original draft; Yeeun Paik, Data curation, Formal analysis, Investigation, Visualization, Methodology; Jennie Hamilton, Conceptualization, Data curation, Formal analysis, Investigation, Methodology; Jingxin Li, Formal analysis, Investigation, Methodology; Karel Kalecky, Data curation, Formal analysis, Investigation, Methodology; Chloe Park, Data curation, Software, Formal analysis, Investigation; Juyeon Lim, Resources, Investigation, Methodology; Sakeenah L Hicks, Data curation, Software, Validation, Methodology; John Karijolich, Software, Investigation, Project administration; Teodoro H Bottiglieri, Data curation, Formal analysis, Supervision, Investigation, Methodology, Project administration; Jeffrey C Rathmell, Conceptualization, Resources, Funding acquisition, Methodology; Denis Mogilenko, Conceptualization, Investigation; Christopher D Scharer, Conceptualization, Data curation, Software, Formal analysis, Supervision, Investigation; Mark R Boothby, Conceptualization, Data curation, Formal analysis, Supervision, Funding acquisition, Methodology, Writing – original draft, Project administration, Writing – review and editing

Author ORCIDs

Sung Hoon Cho https://orcid.org/0000-0002-6463-4032
Yeeun Paik https://orcid.org/0009-0004-9369-2890
Jeffrey C Rathmell https://orcid.org/0000-0002-4106-3396
Denis Mogilenko https://orcid.org/0000-0001-5427-5243
Christopher D Scharer https://orcid.org/0000-0001-7716-8504
Mark R Boothby https://orcid.org/0000-0003-2593-8276

Ethics

This study was conducted in accordance with strict permissions regulated by and requiring prior authorization of the Vanderbilt Institutional Animal Care and Use Committee (IACUC) and strict post-approval daily oversight by the veterinary staff and the Office of Animal Welfare Assurance (OAWA). No surgeries or procedures involving sustained pain or discomfort, or risks of morbidity or mortality, were part of the study.

Peer review material

Version of Record:
Reviewer #2 (Public review): https://doi.org/10.7554/eLife.107627.3.sa1
Reviewer #3 (Public review): https://doi.org/10.7554/eLife.107627.3.sa2
Author response https://doi.org/10.7554/eLife.107627.3.sa3

Reviewed preprint v2
Reviewer #2 (Public review): https://doi.org/10.7554/eLife.107627.2.sa2
Reviewer #3 (Public review): https://doi.org/10.7554/eLife.107627.2.sa1
Author response: https://doi.org/10.7554/eLife.107627.2.sa0
eLife Assessment https://doi.org/10.7554/eLife.107627.2.sa3

Reviewed preprint v1
Reviewer #1 (Public review): https://doi.org/10.7554/eLife.107627.1.sa3

Reviewer #2 (Public review): https://doi.org/10.7554/eLife.107627.1.sa2
Reviewer #3 (Public review): https://doi.org/10.7554/eLife.107627.1.sa1
Author response: https://doi.org/10.7554/eLife.107627.1.sa0
eLife Assessment https://doi.org/10.7554/eLife.107627.1.sa4

Additional files

Supplementary files

MDAR checklist

Data availability

RNA-seq data are publicly available through the Gene Expression Omnibus (GEO) resource of the US National Center for Bio-InformaticsBioinformatics (NCBI), using accession numbers GSE341991 (in vitro cultured B cells during differentiation to Ab-secreting cells) and GSE338789 (flow purified naive and GC B cells). Quantitative data in support of the graphical figure panels have been included as source data files.

The following datasets were generated:

Author(s)	Year	Dataset title	Dataset URL	Database and Identifier
Scharer CD, Boothby M	2026	The role of glutaminolysis and mitochondrial pyruvate import on plasma cell differentiation	https://www.ncbi.nlm.nih.gov/geo/query/acc.cgi?acc=GSE341991	NCBI Gene Expression Omnibus, GSE341991
Scharer CD, Boothby M	2026	The role of GLS1 and MPC2 in germinal center B cell regulation	https://www.ncbi.nlm.nih.gov/geo/query/acc.cgi?acc=GSE338789	NCBI Gene Expression Omnibus, GSE338789

References

Adachi Y, Onodera T, Yamada Y, Daio R, Tsuiji M, Inoue T, Kobayashi K, Kurosaki T, Ato M, Takahashi Y. 2015. Distinct germinal center selection at local sites shapes memory B cell response to viral escape. *The Journal of Experimental Medicine* **212**:1709–1723. DOI: https://doi.org/10.1084/jem.20142284, PMID: 26324444

Akter S, Madhuvilakku R, Kar AK, Nila IS, Liu P, Inuzuka H, Wei W, Hong Y. 2026. Reactive oxygen species (ROS) in cancer: from mechanism to therapeutic implications. *Signal Transduction and Targeted Therapy* **11**:111. DOI: https://doi.org/10.1038/s41392-026-02583-x, PMID: 41881983

Alemán OR, Rosales C. 2023. Human neutrophil Fc gamma receptors: different buttons for different responses. *Journal of Leukocyte Biology* **114**:571–584. DOI: https://doi.org/10.1093/jleuko/qiad080, PMID: 37437115

Altman BJ, Stine ZE, Dang CV. 2016. From Krebs to clinic: glutamine metabolism to cancer therapy. *Nature Reviews. Cancer* **16**:619–634. DOI: https://doi.org/10.1038/nrc.2016.71, PMID: 27492215

Andrews FJ, Griffiths RD. 2002. Glutamine: essential for immune nutrition in the critically ill. *British Journal of Nutrition* **87**:S3–S8. DOI: https://doi.org/10.1079/BJN2001451

Asao H, Okuyama C, Kumaki S, Ishii N, Tsuchiya S, Foster D, Sugamura K. 2001. Cutting edge: the common gamma-chain is an indispensable subunit of the IL-21 receptor complex. *Journal of Immunology* **167**:1–5. DOI: https://doi.org/10.4049/jimmunol.167.1.1, PMID: 11418623

Avery DT, Deenick EK, Ma CS, Suryani S, Simpson N, Chew GY, Chan TD, Palendira U, Bustamante J, Boisson-Dupuis S, Choo S, Bleasel KE, Peake J, King C, French MA, Engelhard D, Al-Hajjar S, Al-Muhsen S, Magdorf K, Roesler J, et al. 2010. B cell-intrinsic signaling through IL-21 receptor and STAT3 is required for establishing long-lived antibody responses in humans. *The Journal of Experimental Medicine* **207**:155–171. DOI: https://doi.org/10.1084/jem.20091706, PMID: 20048285

Banchereau J, Pascual V. 2006. Type I interferon in systemic lupus erythematosus and other autoimmune diseases. *Immunity* **25**:383–392. DOI: https://doi.org/10.1016/j.immuni.2006.08.010, PMID: 16979570

Barwick BG, Scharer CD, Bally APR, Boss JM. 2016. Plasma cell differentiation is coupled to division-dependent DNA hypomethylation and gene regulation. *Nature Immunology* **17**:1216–1225. DOI: https://doi.org/10.1038/ni.3519, PMID: 27500631

Benson MJ, Erickson LD, Gleeson MW, Noelle RJ. 2007. Affinity of antigen encounter and other early B-cell signals determine B-cell fate. *Current Opinion in Immunology* **19**:275–280. DOI: https://doi.org/10.1016/j.coi.2007.04.009, PMID: 17433651

Bhattacharya D. 2022. Instructing durable humoral immunity for COVID-19 and other vaccinable diseases. *Immunity* **55**:945–964. DOI: https://doi.org/10.1016/j.immuni.2022.05.004, PMID: 35637104

Bierling TEH, Gumann A, Ottmann SR, Schulz SR, Weckwerth L, Thomas J, Gessner A, Wichert M, Kuwert F, Rost F, Hauke M, Freudenreich T, Mielenz D, Jäck H-M, Pracht K. 2024. GLUT1-mediated glucose import in B cells is critical for anaplerotic balance and humoral immunity. *Cell Reports* **43**:113739. DOI: https://doi.org/10.1016/j.celrep.2024.113739

Bonanni A, Vaglio A, Bruschi M, Sinico RA, Cavagna L, Moroni G, Franceschini F, Allegri L, Pratesi F, Migliorini P, Candiano G, Pesce G, Ravelli A, Puppo F, Martini A, Tincani A, Ghiggeri GM. 2015. Multi-antibody composition in lupus nephritis: isotype and antigen specificity make the difference. *Autoimmunity Reviews* **14**:692–702. DOI: https://doi.org/10.1016/j.autrev.2015.04.004, PMID: 25888464

Boothby MR, Hodges E, Thomas JW. 2019. Molecular regulation of peripheral B cells and their progeny in immunity. *Genes & Development* **33**:26–48. DOI: https://doi.org/10.1101/gad.320192.118, PMID: 30602439

Boothby MR, Brookens SK, Raybuck AL, Cho SH. 2022. Supplying the trip to antibody production—nutrients, signaling, and the programming of cellular metabolism in the mature B lineage. *Cellular & Molecular Immunology* **19**:352–369. DOI: https://doi.org/10.1038/s41423-021-00782-w

Brookens SK, Cho SH, Paik Y, Meyer K, Raybuck AL, Park C, Greenwood DL, Rathmell JC, Boothby MR. 2024. Plasma cell differentiation, antibody quality, and initial germinal center B cell population depend on glucose influx rate. *Journal of Immunology* **212**:43–56. DOI: https://doi.org/10.4049/jimmunol.2200756, PMID: 37955416

Butturini E, Carcereri de Prati A, Mariotto S. 2020. Redox regulation of STAT1 and STAT3 signaling. *International Journal of Molecular Sciences* **21**:7034. DOI: https://doi.org/10.3390/ijms21197034, PMID: 32987855

Caielli S, Wan Z, Pascual V. 2023. Systemic lupus erythematosus pathogenesis: interferon and beyond. *Annual Review of Immunology* **41**:533–560. DOI: https://doi.org/10.1146/annurev-immunol-101921-042422, PMID: 36854182

Caro-Maldonado A, Wang R, Nichols AG, Kuraoka M, Milasta S, Sun LD, Gavin AL, Abel ED, Kelsoe G, Green DR, Rathmell JC. 2014. Metabolic reprogramming is required for antibody production that is suppressed in anergic but exaggerated in chronically BAFF-exposed B cells. *Journal of Immunology* **192**:3626–3636. DOI: https://doi.org/10.4049/jimmunol.1302062, PMID: 24616478

Celhar T, Magalhães R, Fairhurst AM. 2012. TLR7 and TLR9 in SLE: when sensing self goes wrong. *Immunologic Research* **53**:58–77. DOI: https://doi.org/10.1007/s12026-012-8270-1

Chan TD, Gatto D, Wood K, Camidge T, Basten A, Brink R. 2009. Antigen affinity controls rapid T-dependent antibody production by driving the expansion rather than the differentiation or extrafollicular migration of early plasmablasts. *Journal of Immunology* **183**:3139–3149. DOI: https://doi.org/10.4049/jimmunol.0901690, PMID: 19666691

Chang C-H, Qiu J, O'Sullivan D, Buck MD, Noguchi T, Curtis JD, Chen Q, Gindin M, Gubin MM, van der Windt GJW, Tonc E, Schreiber RD, Pearce EJ, Pearce EL. 2015. Metabolic competition in the tumor microenvironment is a driver of cancer progression. *Cell* **162**:1229–1241. DOI: https://doi.org/10.1016/j.cell.2015.08.016, PMID: 26321679

Chen D, Wang Y, Manakkat Vijay GK, Fu S, Nash CW, Xu D, He D, Salomonis N, Singh H, Xu H. 2021. Coupled analysis of transcriptome and BCR mutations reveals role of OXPHOS in affinity maturation. *Nature Immunology* **22**:904–913. DOI: https://doi.org/10.1038/s41590-021-00936-y

Chiu H, Jackson LV, Oh KI, Mai A, Ronai ZA, Ruggero D, Fruman DA. 2019. The mTORC1/4E-BP/eIF4E axis promotes antibody class switching in B lymphocytes. *The Journal of Immunology* **202**:579–590. DOI: https://doi.org/10.4049/jimmunol.1800602

Cho SH, Raybuck AL, Stengel K, Wei M, Beck TC, Volanakis E, Thomas JW, Hiebert S, Haase VH, Boothby MR. 2016. Germinal centre hypoxia and regulation of antibody qualities by a hypoxia response system. *Nature* **537**:234–238. DOI: https://doi.org/10.1038/nature19334

Cumano A, Rajewsky K. 1985. Structure of primary anti-(4-hydroxy-3-nitrophenyl)acetyl (NP) antibodies in normal and idiotypically suppressed C57BL/6 mice. *European Journal of Immunology* **15**:512–520. DOI: https://doi.org/10.1002/eji.1830150517, PMID: 3873342

Cunningham AF, Gaspal F, Serre K, Mohr E, Henderson IR, Scott-Tucker A, Kenny SM, Khan M, Toellner K-M, Lane PJL, MacLennan ICM. 2007. *Salmonella* induces a switched antibody response without germinal centers that impedes the extracellular spread of infection . *The Journal of Immunology* **178**:6200–6207. DOI: https://doi.org/10.4049/jimmunol.178.10.6200

D'Avola A, Legrave N, Tajan M, Chakravarty P, Shearer RL, King HW, Kluckova K, Cheung EC, Clear AJ, Gunawan AS, Zhang L, James LK, MacRae JI, Gribben JG, Calado DP, Vousden KH, Riches JC. 2022. PHGDH is required for germinal center formation and is a therapeutic target in MYC-driven lymphoma. *The Journal of Clinical Investigation* **132**:e153436. DOI: https://doi.org/10.1172/JCI153436, PMID: 35316216

Domeier PP, Chodisetti SB, Soni C, Schell SL, Elias MJ, Wong EB, Cooper TK, Kitamura D, Rahman ZSM. 2016. IFN-γ receptor and STAT1 signaling in B cells are central to spontaneous germinal center formation and autoimmunity. *The Journal of Experimental Medicine* **213**:715–732. DOI: https://doi.org/10.1084/jem.20151722, PMID: 27069112

Domeier PP, Chodisetti SB, Schell SL, Kawasawa YI, Fasnacht MJ, Soni C, Rahman ZSM. 2018. B-Cell-Intrinsic Type 1 interferon signaling is crucial for loss of tolerance and the development of autoreactive B cells. *Cell Reports* **24**:406–418. DOI: https://doi.org/10.1016/j.celrep.2018.06.046, PMID: 29996101

Dörner T, Lipsky PE. 2024. The essential roles of memory B cells in the pathogenesis of systemic lupus erythematosus. *Nature Reviews. Rheumatology* **20**:770–782. DOI: https://doi.org/10.1038/s41584-024-01179-5, PMID: 39511302

Duan L, Liu D, Chen H, Mintz MA, Chou MY, Kotov DI, Xu Y, An J, Laidlaw BJ, Cyster JG. 2021. Follicular dendritic cells restrict interleukin-4 availability in germinal centers and foster memory B cell generation. *Immunity* **54**:2256–2272. DOI: https://doi.org/10.1016/j.immuni.2021.08.028, PMID: 34555336

Eckl-Dorna J, Batista FD. 2009. BCR-mediated uptake of antigen linked to TLR9 ligand stimulates B-cell proliferation and antigen-specific plasma cell formation. *Blood* **113**:3969–3977. DOI: https://doi.org/10.1182/blood-2008-10-185421

Edinger AL. 2007. Controlling cell growth and survival through regulated nutrient transporter expression. *The Biochemical Journal* **406**:1–12. DOI: https://doi.org/10.1042/BJ20070490, PMID: 17645414

Edwards DN, Ngwa VM, Raybuck AL, Wang S, Hwang Y, Kim LC, Cho SH, Paik Y, Wang Q, Zhang S, Manning HC, Rathmell JC, Cook RS, Boothby MR, Chen J. 2021. Selective glutamine metabolism inhibition in tumor cells improves antitumor T lymphocyte activity in triple-negative breast cancer. *The Journal of Clinical Investigation* **131**:e140100. DOI: https://doi.org/10.1172/JCI140100, PMID: 33320840

Elgueta R, Benson MJ, de Vries VC, Wasiuk A, Guo Y, Noelle RJ. 2009. Molecular mechanism and function of CD40/CD40L engagement in the immune system. *Immunological Reviews* **229**:152–172. DOI: https://doi.org/10.1111/j.1600-065X.2009.00782.x, PMID: 19426221

Elsner RA, Shlomchik MJ. 2020. Germinal center and extrafollicular B cell responses in vaccination, immunity, and autoimmunity. *Immunity* **53**:1136–1150. DOI: https://doi.org/10.1016/j.immuni.2020.11.006, PMID: 33326765

Ettinger R, Sims GP, Fairhurst A-M, Robbins R, da Silva YS, Spolski R, Leonard WJ, Lipsky PE. 2005. IL-21 induces differentiation of human naive and memory B cells into antibody-secreting plasma cells. *Journal of Immunology* **175**:7867–7879. DOI: https://doi.org/10.4049/jimmunol.175.12.7867, PMID: 16339522

Eyer K, Doineau RCL, Castrillon CE, Briseño-Roa L, Menrath V, Mottet G, England P, Godina A, Brient-Litzler E, Nizak C, Jensen A, Griffiths AD, Bibette J, Bruhns P, Baudry J. 2017. Single-cell deep phenotyping of IgG-secreting cells for high-resolution immune monitoring. *Nature Biotechnology* **35**:977–982. DOI: https://doi.org/10.1038/nbt.3964, PMID: 28892076

Eyer K, Castrillon C, Chenon G, Bibette J, Bruhns P, Griffiths AD, Baudry J. 2020. The quantitative assessment of the secreted IgG repertoire after recall to evaluate the quality of immunizations. *Journal of Immunology* **205**:1176–1184. DOI: https://doi.org/10.4049/jimmunol.2000112, PMID: 32669311

Farmer H, McCabe N, Lord CJ, Tutt ANJ, Johnson DA, Richardson TB, Santarosa M, Dillon KJ, Hickson I, Knights C, Martin NMB, Jackson SP, Smith GCM, Ashworth A. 2005. Targeting the DNA repair defect in BRCA mutant cells as a therapeutic strategy. *Nature* **434**:917–921. DOI: https://doi.org/10.1038/nature03445, PMID: 15829967

Fillatreau S, Manfroi B, Dörner T. 2021. Toll-like receptor signalling in B cells during systemic lupus erythematosus. *Nature Reviews. Rheumatology* **17**:98–108. DOI: https://doi.org/10.1038/s41584-020-00544-4, PMID: 33339987

Fontaine E. 2018. Metformin-induced mitochondrial complex I inhibition: facts, uncertainties, and consequences. *Frontiers in Endocrinology* **9**:753. DOI: https://doi.org/10.3389/fendo.2018.00753, PMID: 30619086

Fox J, Weisberg S. 2018. *An R Companion to Applied Regression*. SAGE Publications.

Geyer CE, Mes L, Newling M, den Dunnen J, Hoepel W. 2021. Physiological and pathological inflammation induced by antibodies and pentraxins. *Cells* **10**:1175. DOI: https://doi.org/10.3390/cells10051175, PMID: 34065953

Golias T, Papandreou I, Sun R, Kumar B, Brown NV, Swanson BJ, Pai R, Jaitin D, Le QT, Teknos TN, Denko NC. 2016. Hypoxic repression of pyruvate dehydrogenase activity is necessary for metabolic reprogramming and growth of model tumours. *Scientific Reports* **6**:31146. DOI: https://doi.org/10.1038/srep31146, PMID: 27498883

Good-Jacobson KL, Shlomchik MJ. 2010. Plasticity and heterogeneity in the generation of memory B cells and long-lived plasma cells: the influence of germinal center interactions and dynamics. *Journal of Immunology* **185**:3117–3125. DOI: https://doi.org/10.4049/jimmunol.1001155, PMID: 20814029

Green NM, Marshak-Rothstein A. 2011. Toll-like receptor driven B cell activation in the induction of systemic autoimmunity. *Seminars in Immunology* **23**:106–112. DOI: https://doi.org/10.1016/j.smim.2011.01.016, PMID: 21306913

Hamilton JA, Wu Q, Yang P, Luo B, Liu S, Hong H, Li J, Walter MR, Fish EN, Hsu HC, Mountz JD. 2017. Cutting edge: endogenous IFN-β regulates survival and development of transitional B cells. *Journal of Immunology* **199**:2618–2623. DOI: https://doi.org/10.4049/jimmunol.1700888, PMID: 28904124

Haslene-Hox H, Oveland E, Berg KC, Kolmannskog O, Woie K, Salvesen HB, Tenstad O, Wiig H. 2011. A new method for isolation of interstitial fluid from human solid tumors applied to proteomic analysis of ovarian carcinoma tissue. *PLOS ONE* **6**:e19217. DOI: https://doi.org/10.1371/journal.pone.0019217, PMID: 21541282

Higgs BW, Liu Z, White B, Zhu W, White WI, Morehouse C, Brohawn P, Kiener PA, Richman L, Fiorentino D, Greenberg SA, Jallal B, Yao Y. 2011. Patients with systemic lupus erythematosus, myositis, rheumatoid arthritis and scleroderma share activation of a common type I interferon pathway. *Annals of the Rheumatic Diseases* **70**:2029–2036. DOI: https://doi.org/10.1136/ard.2011.150326, PMID: 21803750

Ho PC, Bihuniak JD, Macintyre AN, Staron M, Liu X, Amezquita R, Tsui YC, Cui G, Micevic G, Perales JC, Kleinstein SH, Abel ED, Insogna KL, Feske S, Locasale JW, Bosenberg MW, Rathmell JC, Kaech SM. 2015. Phosphoenolpyruvate is a metabolic checkpoint of anti-tumor T cell responses. *Cell* **162**:1217–1228. DOI: https://doi.org/10.1016/j.cell.2015.08.012, PMID: 26321681

Ikeda H, Old LJ, Schreiber RD. 2002. The roles of IFNγ in protection against tumor development and cancer immunoediting. *Cytokine & Growth Factor Reviews* **13**:95–109. DOI: https://doi.org/10.1016/S1359-6101(01)00038-7

Inoue T, Kurosaki T. 2024. Memory B cells. *Nature Reviews. Immunology* **24**:5–17. DOI: https://doi.org/10.1038/s41577-023-00897-3, PMID: 37400644

Ise W, Kurosaki T. 2019. Plasma cell differentiation during the germinal center reaction. *Immunological Reviews* **288**:64–74. DOI: https://doi.org/10.1111/imr.12751, PMID: 30874351

Jellusova J, Cato MH, Apgar JR, Ramezani-Rad P, Leung CR, Chen C, Richardson AD, Conner EM, Benschop RJ, Woodgett JR, Rickert RC. 2017. Gsk3 is a metabolic checkpoint regulator in B cells. *Nature Immunology* **18**:303–312. DOI: https://doi.org/10.1038/ni.3664, PMID: 28114292

Johnson MO, Siska PJ, Contreras DC, Rathmell JC. 2016. Nutrients and the microenvironment to feed a T cell army. *Seminars in Immunology* **28**:505–513. DOI: https://doi.org/10.1016/j.smim.2016.09.003, PMID: 27712958

Johnson MO, Wolf MM, Madden MZ, Andrejeva G, Sugiura A, Contreras DC, Maseda D, Liberti MV, Paz K, Kishton RJ, Johnson ME, de Cubas AA, Wu P, Li G, Zhang Y, Newcomb DC, Wells AD, Restifo NP, Rathmell WK, Locasale JW, et al. 2018. Distinct regulation of Th17 and Th1 cell differentiation by glutaminase-dependent metabolism. *Cell* **175**:1780–1795. DOI: https://doi.org/10.1016/j.cell.2018.10.001, PMID: 30392958

Jones DD, Gaudette BT, Wilmore JR, Chernova I, Bortnick A, Weiss BM, Allman D. 2016. mTOR has distinct functions in generating versus sustaining humoral immunity. *Journal of Clinical Investigation* **126**:4250–4261. DOI: https://doi.org/10.1172/JCI86504

Kato Y, Abbott RK, Freeman BL, Haupt S, Groschel B, Silva M, Menis S, Irvine DJ, Schief WR, Crotty S. 2020. Multifaceted effects of antigen valency on B cell response composition and differentiation in vivo. *Immunity* **53**:548–563. DOI: https://doi.org/10.1016/j.immuni.2020.08.001, PMID: 32857950

Khalil AM, Cambier JC, Shlomchik MJ. 2012. B cell receptor signal transduction in the GC is short-circuited by high phosphatase activity. *Science* **336**:1178–1181. DOI: https://doi.org/10.1126/science.1213368, PMID: 22555432

Kim J, Won JS, Singh AK, Sharma AK, Singh I. 2014. STAT3 regulation by S-nitrosylation: implication for inflammatory disease. *Antioxidants & Redox Signaling* **20**:2514–2527. DOI: https://doi.org/10.1089/ars.2013.5223

King IL, Mohrs M. 2009. IL-4–producing CD4+ T cells in reactive lymph nodes during helminth infection are T follicular helper cells. *Journal of Experimental Medicine* **206**:1001–1007. DOI: https://doi.org/10.1084/jem.20090313

Kiritsy MC, McCann K, Mott D, Holland SM, Behar SM, Sassetti CM, Olive AJ. 2021. Mitochondrial respiration contributes to the interferon gamma response in antigen-presenting cells. *eLife* **10**:e65109. DOI: https://doi.org/10.7554/eLife.65109, PMID: 34726598

Klysz D, Tai X, Robert PA, Craveiro M, Cretenet G, Oburoglu L, Mongellaz C, Floess S, Fritz V, Matias MI, Yong C, Surh N, Marie JC, Huehn J, Zimmermann V, Kinet S, Dardalhon V, Taylor N. 2015. Glutamine-dependent α-ketoglutarate production regulates the balance between T helper 1 cell and regulatory T cell generation. *Science Signaling* **8**:ra97. DOI: https://doi.org/10.1126/scisignal.aab2610, PMID: 26420908

Kometani K, Nakagawa R, Shinnakasu R, Kaji T, Rybouchkin A, Moriyama S, Furukawa K, Koseki H, Takemori T, Kurosaki T. 2013. Repression of the transcription factor Bach2 contributes to predisposition of IgG1 memory B cells toward plasma cell differentiation. *Immunity* **39**:136–147. DOI: https://doi.org/10.1016/j.immuni.2013.06.011, PMID: 23850379

Kurosaki T. 1999. Genetic analysis of B cell antigen receptor signaling. *Annual Review of Immunology* **17**:555–592. DOI: https://doi.org/10.1146/annurev.immunol.17.1.555

Kwak K, Akkaya M, Pierce SK. 2019. B cell signaling in context. *Nature Immunology* **20**:963–969. DOI: https://doi.org/10.1038/s41590-019-0427-9, PMID: 31285625

Lam WY, Becker AM, Kennerly KM, Wong R, Curtis JD, Llufrio EM, McCommis KS, Fahrmann J, Pizzato HA, Nunley RM, Lee J, Wolfgang MJ, Patti GJ, Finck BN, Pearce EL, Bhattacharya D. 2016. Mitochondrial pyruvate import promotes long-term survival of antibody-secreting plasma cells. *Immunity* **45**:60–73. DOI: https://doi.org/10.1016/j.immuni.2016.06.011, PMID: 27396958

Larsen S, Rabøl R, Hansen CN, Madsbad S, Helge JW, Dela F. 2012. Metformin-treated patients with type 2 diabetes have normal mitochondrial complex I respiration. *Diabetologia* **55**:443–449. DOI: https://doi.org/10.1007/s00125-011-2340-0, PMID: 22009334

Laumont CM, Banville AC, Gilardi M, Hollern DP, Nelson BH. 2022. Tumour-infiltrating B cells: immunological mechanisms, clinical impact and therapeutic opportunities. *Nature Reviews. Cancer* **22**:414–430. DOI: https://doi.org/10.1038/s41568-022-00466-1, PMID: 35393541

Leach S, Shinnakasu R, Adachi Y, Momota M, Makino-Okamura C, Yamamoto T, Ishii KJ, Fukuyama H, Takahashi Y, Kurosaki T. 2019. Requirement for memory B-cell activation in protection from heterologous influenza virus reinfection. *International Immunology* **31**:771–779. DOI: https://doi.org/10.1093/intimm/dxz049, PMID: 31231764

Lee CH, Motzer R, Emamekhoo H, Matrana M, Percent I, Hsieh JJ, Hussain A, Vaishampayan U, Liu S, McCune S, Patel V, Shaheen M, Bendell J, Fan AC, Gartrell BA, Goodman OB, Nikolinakos PG, Kalebasty AR, Zakharia Y, Zhang Z, et al. 2022. Telaglenastat plus everolimus in advanced renal cell carcinoma: a randomized, double-blinded, placebo-controlled, phase II ENTRATA trial. *Clinical Cancer Research* **28**:3248–3255. DOI: https://doi.org/10.1158/1078-0432.CCR-22-0061, PMID: 35576438

Li N, Ragheb K, Lawler G, Sturgis J, Rajwa B, Melendez JA, Robinson JP. 2003. Mitochondrial complex I inhibitor rotenone induces apoptosis through enhancing mitochondrial reactive oxygen species production. *The Journal of Biological Chemistry* **278**:8516–8525. DOI: https://doi.org/10.1074/jbc.M210432200, PMID: 12496265

Li L, Cheung SH, Evans EL, Shaw PE. 2010. Modulation of gene expression and tumor cell growth by redox modification of STAT3. *Cancer Research* **70**:8222–8232. DOI: https://doi.org/10.1158/0008-5472.CAN-10-0894, PMID: 20807804

Li L, Feng C, Qin J, Li D, Liu M, Han S, Zheng B. 2021. Regulation of humoral immune response by HIF-1α-dependent metabolic reprogramming of the germinal center reaction. *Cellular Immunology* **367**:104409. DOI: https://doi.org/10.1016/j.cellimm.2021.104409, PMID: 34246872

Li M, Zhou X, Li Y, Zhu X, Li Y, Hitosugi T, Zeng H. 2024. CPT2-mediated fatty acid oxidation is dispensable for humoral immunity. *Journal of Immunology* **213**:1139–1149. DOI: https://doi.org/10.4049/jimmunol.2400285, PMID: 39258879

Limonciel A. 2020. Translate metabolomics & lipidomics into knowledge. *MetaboNews* **10**:3–5.

Liu P-S, Wang H, Li X, Chao T, Teav T, Christen S, Di Conza G, Cheng W-C, Chou C-H, Vavakova M, Muret C, Debackere K, Mazzone M, Huang H-D, Fendt S-M, Ivanisevic J, Ho P-C. 2017. α-ketoglutarate orchestrates macrophage activation through metabolic and epigenetic reprogramming. *Nature Immunology* **18**:985–994. DOI: https://doi.org/10.1038/ni.3796

Lu LL, Suscovich TJ, Fortune SM, Alter G. 2018. Beyond binding: antibody effector functions in infectious diseases. *Nature Reviews. Immunology* **18**:46–61. DOI: https://doi.org/10.1038/nri.2017.106, PMID: 29063907

Luan Y, Dai P, Wang Y, Liu J, Cai Y, Min Q, Zhang R, Hu Z, Wen Z, Dong L, Hu W, Li F, Yeap LS, Zou J, Shen Q, Xu H, Rao J, Meng FL, Wang JY. 2026. IgG2c subclass dominance drives fatal lupus-like nephritis via FcγR and complement activation. *Cell Reports* **45**:116775. DOI: https://doi.org/10.1016/j.celrep.2025.116775

MacLean AJ, Deimel LP, Zhou P, ElTanbouly MA, Merkenschlager J, Ramos V, Santos GS, Hägglöf T, Mayer CT, Hernandez B, Gazumyan A, Nussenzweig MC. 2025. Affinity maturation of antibody responses is mediated by differential plasma cell proliferation. *Science* **387**:413–420. DOI: https://doi.org/10.1126/science.adr6896, PMID: 39700316

Marshall AJ, Niiro H, Yun TJ, Clark EA. 2000. Regulation of B-cell activation and differentiation by the phosphatidylinositol 3-kinase and phospholipase Cγ pathways. *Immunological Reviews* **176**:30–46. DOI: https://doi.org/10.1034/j.1600-065X.2000.00611.x

McGettigan SE, Debes GF. 2021. Immunoregulation by antibody secreting cells in inflammation, infection, and cancer. *Immunological Reviews* **303**:103–118. DOI: https://doi.org/10.1111/imr.12991, PMID: 34145601

Mesin L, Schiepers A, Ersching J, Barbulescu A, Cavazzoni CB, Angelini A, Okada T, Kurosaki T, Victora GD. 2020. Restricted clonality and limited germinal center reentry characterize memory B cell reactivation by boosting. *Cell* **180**:92–106. DOI: https://doi.org/10.1016/j.cell.2019.11.032, PMID: 31866068

Mesin L, Hobbs A, Shen JJ, Pae J, Schiepers A, Abrahamse N, Muramatsu H, Tam YK, Pardi N, Victora GD. 2026. Clonal dynamics of germinal center refueling by secondary immunization. *bioRxiv*. DOI: https://doi.org/10.64898/2026.05.26.728008

Mitchell TC, Hildeman D, Kedl RM, Teague TK, Schaefer BC, White J, Zhu Y, Kappler J, Marrack P. 2001. Immunological adjuvants promote activated T cell survival via induction of Bcl-3. *Nature Immunology* **2**:397–402. DOI: https://doi.org/10.1038/87692, PMID: 11323692

Mukherjee S, Zhu J, Zikherman J, Parameswaran R, Kadlecek TA, Wang Q, Au-Yeung B, Ploegh H, Kuriyan J, Das J, Weiss A. 2013. Monovalent and multivalent ligation of the B cell receptor exhibit differential dependence upon Syk and Src family kinases. *Science Signaling* **6**:ra1. DOI: https://doi.org/10.1126/scisignal.2003220, PMID: 23281368

Müller F, Taubmann J, Bucci L, Wilhelm A, Bergmann C, Völkl S, Aigner M, Rothe T, Minopoulou I, Tur C, Knitza J, Kharboutli S, Kretschmann S, Vasova I, Spoerl S, Reimann H, Munoz L, Gerlach RG, Schäfer S, Grieshaber-Bouyer R, et al. 2024. CD19 CAR T-cell therapy in autoimmune disease - a case series with follow-up. *The New England Journal of Medicine* **390**:687–700. DOI: https://doi.org/10.1056/NEJMoa2308917, PMID: 38381673

Nakagawa R, Llorian M, Varsani-Brown S, Chakravarty P, Camarillo JM, Barry D, George R, Blackledge NP, Duddy G, Kelleher NL, Klose RJ, Turner M, Calado DP. 2024. Epi-microRNA mediated metabolic reprogramming counteracts hypoxia to preserve affinity maturation. *Nature Communications* **15**:10516. DOI: https://doi.org/10.1038/s41467-024-54937-0, PMID: 39627218

Nohr CW, Tchervenkov JI, Meakins JL, Christou NV. 1986. Malnutrition and humoral immunity: long-term protein deprivation. *The Journal of Surgical Research* **40**:432–437. DOI: https://doi.org/10.1016/0022-4804(86)90211-8, PMID: 3090370

Olsen NJ, Schleich MA, Karp DR. 2013. Multifaceted effects of hydroxychloroquine in human disease. *Seminars in Arthritis and Rheumatism* **43**:264–272. DOI: https://doi.org/10.1016/j.semarthrit.2013.01.001, PMID: 23481418

Olsen NJ, Karp DR. 2014. Autoantibodies and SLE: the threshold for disease. *Nature Reviews. Rheumatology* **10**:181–186. DOI: https://doi.org/10.1038/nrrheum.2013.184, PMID: 24296678

O'Neil NJ, Bailey ML, Hieter P. 2017. Synthetic lethality and cancer. *Nature Reviews. Genetics* **18**:613–623. DOI: https://doi.org/10.1038/nrg.2017.47, PMID: 28649135

Ozaki K, Spolski R, Feng CG, Qi C-F, Cheng J, Sher A, Morse HC III, Liu C, Schwartzberg PL, Leonard WJ. 2002. A critical role for IL-21 in regulating immunoglobulin production. *Science* **298**:1630–1634. DOI: https://doi.org/10.1126/science.1077002

Paus D, Phan TG, Chan TD, Gardam S, Basten A, Brink R. 2006. Antigen recognition strength regulates the choice between extrafollicular plasma cell and germinal center B cell differentiation. *The Journal of Experimental Medicine* **203**:1081–1091. DOI: https://doi.org/10.1084/jem.20060087, PMID: 16606676

Phan TG, Paus D, Chan TD, Turner ML, Nutt SL, Basten A, Brink R. 2006. High affinity germinal center B cells are actively selected into the plasma cell compartment. *The Journal of Experimental Medicine* **203**:2419–2424. DOI: https://doi.org/10.1084/jem.20061254, PMID: 17030950

Pignarre A, Chatonnet F, Caron G, Haas M, Desmots F, Fest T. 2021. Plasmablasts derive from CD23- activated B cells after the extinction of IL-4/STAT6 signaling and IRF4 induction. *Blood* **137**:1166–1180. DOI: https://doi.org/10.1182/blood.2020005083, PMID: 33150420

Pilati C, Amessou M, Bihl MP, Balabaud C, Nhieu JTV, Paradis V, Nault JC, Izard T, Bioulac-Sage P, Couchy G, Poussin K, Zucman-Rossi J. 2011. Somatic mutations activating STAT3 in human inflammatory hepatocellular adenomas. *The Journal of Experimental Medicine* **208**:1359–1366. DOI: https://doi.org/10.1084/jem.20110283, PMID: 21690253

Pone EJ, Hernandez-Davies JE, Jan S, Silzel E, Felgner PL, Davies DH. 2022. Multimericity amplifies the synergy of BCR and TLR4 for B cell activation and antibody class switching. *Frontiers in Immunology* **13**:882502. DOI: https://doi.org/10.3389/fimmu.2022.882502, PMID: 35663959

Price MJ, Patterson DG, Scharer CD, Boss JM. 2018. Progressive upregulation of oxidative metabolism facilitates plasmablast differentiation to a T-independent antigen. *Cell Reports* **23**:3152–3159. DOI: https://doi.org/10.1016/j.celrep.2018.05.053

Puffer EB, Pontrello JK, Hollenbeck JJ, Kink JA, Kiessling LL. 2007. Activating B cell signaling with defined multivalent ligands. *ACS Chemical Biology* **2**:252–262. DOI: https://doi.org/10.1021/cb600489g, PMID: 17432821

Rajewsky K. 1996. Clonal selection and learning in the antibody system. *Nature* **381**:751–758. DOI: https://doi.org/10.1038/381751a0, PMID: 8657279

Rathmell JC, Townsend SE, Xu JC, Flavell RA, Goodnow CC. 1996. Expansion or elimination of B cells in vivo: dual roles for CD40- and Fas (CD95)-ligands modulated by the B cell antigen receptor. *Cell* **87**:319–329. DOI: https://doi.org/10.1016/s0092-8674(00)81349-5, PMID: 8861915

Raybuck AL, Cho SH, Li J, Rogers MC, Lee K, Williams CL, Shlomchik M, Thomas JW, Chen J, Williams JV, Boothby MR. 2018. B Cell-Intrinsic mTORC1 promotes germinal center-defining transcription factor gene expression, somatic hypermutation, and memory B cell generation in humoral immunity. *Journal of Immunology* **200**:2627–2639. DOI: https://doi.org/10.4049/jimmunol.1701321, PMID: 29531165

Ripperger TJ, Bhattacharya D. 2021. Transcriptional and metabolic control of memory B cells and plasma cells. *Annual Review of Immunology* **39**:345–368. DOI: https://doi.org/10.1146/annurev-immunol-093019-125603, PMID: 33556247

Robinson MJ, Webster RH, Tarlinton DM. 2020. How intrinsic and extrinsic regulators of plasma cell survival might intersect for durable humoral immunity. *Immunological Reviews* **296**:87–103. DOI: https://doi.org/10.1111/imr.12895, PMID: 32592168

Rodríguez-Bayona B, Ramos-Amaya A, López-Blanco R, Campos-Caro A, Brieva JA. 2013. STAT-3 activation by differential cytokines is critical for human in vivo–generated plasma cell survival and Ig secretion. *The Journal of Immunology* **191**:4996–5004. DOI: https://doi.org/10.4049/jimmunol.1301559

Rönnblom L, Eloranta ML. 2013. The interferon signature in autoimmune diseases. *Current Opinion in Rheumatology* **25**:248–253. DOI: https://doi.org/10.1097/BOR.0b013e32835c7e32, PMID: 23249830

Rubtsova K, Rubtsov AV, van Dyk LF, Kappler JW, Marrack P. 2013. T-box transcription factor T-bet, a key player in a unique type of B-cell activation essential for effective viral clearance. *PNAS* **110**:E3216–E3224. DOI: https://doi.org/10.1073/pnas.1312348110

Ruiz-Iglesias A, Mañes S. 2021. The importance of mitochondrial pyruvate carrier in cancer cell metabolism and tumorigenesis. *Cancers* **13**:1488. DOI: https://doi.org/10.3390/cancers13071488, PMID: 33804985

Sadzak I, Schiff M, Gattermeier I, Glinitzer R, Sauer I, Saalmüller A, Yang E, Schaljo B, Kovarik P. 2008. Recruitment of Stat1 to chromatin is required for interferon-induced serine phosphorylation of Stat1 transactivation domain. *PNAS* **105**:8944–8949. DOI: https://doi.org/10.1073/pnas.0801794105, PMID: 18574148

Sarvaria A, Madrigal JA, Saudemont A. 2017. B cell regulation in cancer and anti-tumor immunity. *Cellular & Molecular Immunology* **14**:662–674. DOI: https://doi.org/10.1038/cmi.2017.35, PMID: 28626234

Scharer CD, Patterson DG, Mi T, Price MJ, Hicks SL, Boss JM. 2020. Antibody-secreting cell destiny emerges during the initial stages of B-cell activation. *Nature Communications* **11**:3989. DOI: https://doi.org/10.1038/s41467-020-17798-x, PMID: 32778653

Schiepers A, Van't Wout MFL, Hobbs A, Mesin L, Victora GD. 2024. Opposing effects of pre-existing antibody and memory T cell help on the dynamics of recall germinal centers. *Immunity* **57**:1618–1628. DOI: https://doi.org/10.1016/j.immuni.2024.05.009, PMID: 38838672

Shapiro-Shelef M, Calame K. 2005. Regulation of plasma-cell development. *Nature Reviews. Immunology* **5**:230–242. DOI: https://doi.org/10.1038/nri1572, PMID: 15738953

Shapiro-Shelef M, Lin K-I, Savitsky D, Liao J, Calame K. 2005. Blimp-1 is required for maintenance of long-lived plasma cells in the bone marrow. *The Journal of Experimental Medicine* **202**:1471–1476. DOI: https://doi.org/10.1084/jem.20051611, PMID: 16314438

Sugiura A, Andrejeva G, Voss K, Heintzman DR, Xu X, Madden MZ, Ye X, Beier KL, Chowdhury NU, Wolf MM, Young AC, Greenwood DL, Sewell AE, Shahi SK, Freedman SN, Cameron AM, Foerch P, Bourne T, Garcia-Canaveras JC, Karijolich J, et al. 2022. MTHFD2 is a metabolic checkpoint controlling effector and

regulatory T cell fate and function. *Immunity* **55**:65–81.. DOI: https://doi.org/10.1016/j.immuni.2021.10.011, PMID: 34767747

Suurmond J, Diamond B. 2015. Autoantibodies in systemic autoimmune diseases: specificity and pathogenicity. *The Journal of Clinical Investigation* **125**:2194–2202. DOI: https://doi.org/10.1172/JCI78084, PMID: 25938780

Tao L, Lemoff A, Wang G, Zarek C, Lowe A, Yan N, Reese TA. 2020. Reactive oxygen species oxidize STING and suppress interferon production. *eLife* **9**:e57837. DOI: https://doi.org/10.7554/eLife.57837, PMID: 32886065

Taubmann J, Müller F, Yalcin Mutlu M, Völkl S, Aigner M, Bozec A, Mackensen A, Grieshaber-Bouyer R, Schett G. 2024. CD19 chimeric antigen receptor T cell treatment: unraveling the role of B cells in systemic lupus erythematosus. *Arthritis & Rheumatology* **76**:497–504. DOI: https://doi.org/10.1002/art.42784, PMID: 38114423

Taylor AK, Cao W, Vora KP, Cruz JDL, Shieh W-J, Zaki SR, Katz JM, Sambhara S, Gangappa S. 2013. Protein energy malnutrition decreases immunity and increases susceptibility to influenza infection in mice. *The Journal of Infectious Diseases* **207**:501–510. DOI: https://doi.org/10.1093/infdis/jis527

Tsokos GC, Lo MS, Costa Reis P, Sullivan KE. 2016. New insights into the immunopathogenesis of systemic lupus erythematosus. *Nature Reviews. Rheumatology* **12**:716–730. DOI: https://doi.org/10.1038/nrrheum.2016.186, PMID: 27872476

Tukey JW. 1977. *Exploratory Data Analysis*. Addison-Wesley.

Urbanczyk S, Baris OR, Hofmann J, Taudte RV, Guegen N, Golombek F, Castiglione K, Meng X, Bozec A, Thomas J, Weckwerth L, Mougiakakos D, Schulz SR, Schuh W, Schlötzer-Schrehardt U, Steinmetz TD, Brodesser S, Wiesner RJ, Mielenz D. 2022. Mitochondrial respiration in B lymphocytes is essential for humoral immunity by controlling the flux of the TCA cycle. *Cell Reports* **39**:110912. DOI: https://doi.org/10.1016/j.celrep.2022.110912

Victora GD, Nussenzweig MC. 2022. Germinal centers. *Annual Review of Immunology* **40**:413–442. DOI: https://doi.org/10.1146/annurev-immunol-120419-022408, PMID: 35113731

Vijay R, Guthmiller JJ, Sturtz AJ, Surette FA, Rogers KJ, Sompallae RR, Li F, Pope RL, Chan J-A, de Labastida Rivera F, Andrew D, Webb L, Maury WJ, Xue H-H, Engwerda CR, McCarthy JS, Boyle MJ, Butler NS. 2020. Infection-induced plasmablasts are a nutrient sink that impairs humoral immunity to malaria. *Nature Immunology* **21**:790–801. DOI: https://doi.org/10.1038/s41590-020-0678-5, PMID: 32424361

Weisel FJ, Mullett SJ, Elsner RA, Menk AV, Trivedi N, Luo W, Wikenheiser D, Hawse WF, Chikina M, Smita S, Conter LJ, Joachim SM, Wendell SG, Jurczak MJ, Winkler TH, Delgoffe GM, Shlomchik MJ. 2020. Germinal center B cells selectively oxidize fatty acids for energy while conducting minimal glycolysis. *Nature Immunology* **21**:331–342. DOI: https://doi.org/10.1038/s41590-020-0598-4

Wong R, Belk JA, Govero J, Uhrlaub JL, Reinartz D, Zhao H, Errico JM, D'Souza L, Ripperger TJ, Nikolich-Zugich J, Shlomchik MJ, Satpathy AT, Fremont DH, Diamond MS, Bhattacharya D. 2020. Affinity-restricted memory B cells dominate recall responses to heterologous flaviviruses. *Immunity* **53**:1078–1094.. DOI: https://doi.org/10.1016/j.immuni.2020.09.001

Yazicioglu YF, Marin E, Sandhu C, Galiani S, Raza IGA, Ali M, Kronsteiner B, Compeer EB, Attar M, Dunachie SJ, Dustin ML, Clarke AJ. 2023. Dynamic mitochondrial transcription and translation in B cells control germinal center entry and lymphomagenesis. *Nature Immunology* **24**:991–1006. DOI: https://doi.org/10.1038/s41590-023-01484-3, PMID: 37095377

Young CD, Lewis AS, Rudolph MC, Ruehle MD, Jackman MR, Yun UJ, Ilkun O, Pereira R, Abel ED, Anderson SM. 2011. Modulation of glucose transporter 1 (GLUT1) expression levels alters mouse mammary tumor cell growth in vitro and in vivo. *PLOS ONE* **6**:e23205. DOI: https://doi.org/10.1371/journal.pone.0023205, PMID: 21826239

Zangari J, Petrelli F, Maillot B, Martinou JC. 2020. The multifaceted pyruvate metabolism: role of the mitochondrial pyruvate carrier. *Biomolecules* **10**:1068. DOI: https://doi.org/10.3390/biom10071068, PMID: 32708919

Appendix 1

Appendix 1—key resources table

Reagent type (species) or resource	Designation	Source or reference	Identifiers	Additional information
Genetic reagent (*Mus musculus*)	C57/Bl6 (B6) – *Gls1* $^{f/f}$	Rathmell (VUMC, now U of Chicago); ***Johnson et al., 2018***	none	conditional loss-of-function allele encoding GLS
Genetic reagent (*Mus musculus*)	C57/Bl6 (B6) – *Slc2a1* $^{f/f}$	Rathmell (VUMC, now U of Chicago); Jackson Lab; ***Young et al., 2011***	none	conditional loss-of-function allele encoding GLUT1
Genetic reagent (*Mus musculus*)	C56/Bl6(B6) – *Mpc2* $^{f/f}$	Bhattacharya (U of AZ); ***Lam et al., 2016***	none	conditional loss-of-function allele encoding MPC2
Genetic reagent (*Mus musculus*)	B6 - *Rosa26-CreER*^{T2}	Ludwig (Ohio State Univ.); ***Shapiro-Shelef et al., 2005***	none	conditionally active recombinase
Genetic reagent (*Mus musculus*)	B6 - *huCD20-CreER*^{T2}	Shlomchik (Yale Univ; now @ UPMC); ***Khalil et al., 2012***	none	B cell-specific conditionally active recombinase
Peptide, recombinant protein	NP-ovalbumin	Biosearch Tech - now Fina Bio; ***Victora and Nussenzweig, 2022***	**Catalog #** N5051-100	
Peptide, recombinant protein	NP(~20)-BSA	Biosearch Tech → Fina Bio	**Catalog #** N5050H	
Peptide, recombinant protein	NP2-PSA	Biosearch Tech → Fina Bio	**Catalog #** N5050L	
Antibody	Anti-GLS1 Ab (rabbit monoclonal)	Invitrogen	**Catalog #** 701965	WB (1:1000)
Antibody	Anti-pSTAT1-Y701 Ab (rabbit monoclonal)	Cell Signaling Technologies	**Catalog #** 9167	WB (1:1000)
Antibody	Anti-pSTAT1-S727 Ab (rabbit monoclonal)	Cell Signaling Technologies	**Catalog #** 8826	WB (1:1000)
Antibody	Anti-pSTAT3-Y705 Ab (rabbit monoclonal)	Cell Signaling Technologies	Catalog # 9145	WB (1:1000)
Antibody	Anti-pJak1-Y1034/1035 Ab (rabbit monoclonal)	Cell Signaling Technologies	Catalog # 74129	WB (1:1000)
Antibody	Anti-mouse β-Actin Ab (mouse monoclonal)	Santa Cruz Biotech	Catalog # sc-517582	WB (1:2000)
Antibody	Anti-Cyclophilin B Ab (rabbit polyclonal)	Millipore Sigma	Catalog # SAB4200201	WB (1:5000)
Antibody	Anti-mouse GL7-FITC (rat monoclonal)	BD Biosciences	Catalog # 562080; RRID:AB_10894953	FACS (1:250) IHC (1:100)
Antibody	Anti-mouse IgM-FITC (rat monoclonal)	BD Biosciences	**Catalog #** 553437; RRID:AB_394857	FACS (1:500)
Antibody	Anti-mouse GL7-PE (rat monoclonal)	BD Biosciences	**Catalog #** 561530; RRID:AB_10715834	FACS (1:250)

Appendix 1 Continued on next page

Appendix 1 Continued

Reagent type (species) or resource	Designation	Source or reference	Identifiers	Additional information
Antibody	Anti-mouse IgD-PE (rat monoclonal)	eBioscience	Catalog # 12-5993-83	FACS (1:500) IHC (1:200)
Antibody	Anti-mouse PD1-PE (rat monoclonal)	BD Biosciences	**Catalog #** 568260 RRID:AB_2916860	FACS (1:500)
Antibody	Anti-mouse CD21-BV510 (rat monoclonal)	BioLegends	**Catalog #** 123437; RRID:AB_2876441	FACS (1:500)
Antibody	Anti-mouse TCRb-PE-cy5 (hamster monoclonal)	Invitrogen	**Catalog #** 15-5961-82	FACS (1:500)
Chemical compound	Ghost Dye-Violet 450	Tonbo Bioscience	**Catalog #** 13–0868 T500	FACS (1:500)
Chemical compound	Ghost Dye-Violet 510	Tonbo Bioscience	**Catalog #** 13–0870 T100	FACS (1:500)
Antibody	Anti-mouse CD11b-PerCP (rat monoclonal)	Tonbo Bioscience	**Catalog #** 65–0112 U025	FACS (1:500)
Antibody	Anti-mouse CD11c-PerCP (rat monoclonal)	Tonbo Bioscience	**Catalog #** 65–0114 U025	FACS (1:500)
Antibody	Anti-mouse F4/80-PerCP (rat monoclonal)	Tonbo Bioscience	**Catalog #** 65–4801 U025	FACS (1:500)
Antibody	Anti-mouse Gr1-PerCP (rat monoclonal)	Tonbo Bioscience	**Catalog #** 67–5931 U025	FACS (1:500)
Antibody	Anti-mouse CD19-APC (rat monoclonal)	Tonbo Bioscience	**Catalog #** 20–0193 U025	FACS (1:500)
Antibody	Anti-mouse CD19-PE-Cy7 (rat monoclonal)	Tonbo Bioscience	**Catalog #** 60–0193 U025	FACS (1:500)
Antibody	Anti-mouse B220-APC-Cy7 (rat monoclonal)	Tonbo Bioscience	**Catalog #** 25–0452 U025	FACS (1:500)
Antibody	Anti-mouse CD43-APC (rat monoclonal)	BD Biosciences	**Catalog #** 560663; RRID:AB_1727479	FACS (1:500)
Antibody	Anti-mouse CXCR4-APC (rat monoclonal)	BD Biosciences	**Catalog # 558644**; RRID:AB_1645219	FACS (1:250)
Antibody	Anti-mouse CD38-eFlour 450 (rat monoclonal)	eBioscience	**Catalog #** 48-0388-42	FACS (1:500)
Antibody	Anti-mouse CD95-Biotin (hamster monoclonal)	BD Bioscience	**Catalog # 554256**; RRID:AB_395328	FACS (1:500)

Appendix 1 Continued on next page

Appendix 1 Continued

Reagent type (species) or resource	Designation	Source or reference	Identifiers	Additional information
Antibody	Anti-mouse CD35-Biotin (rat monoclonal)	BD Bioscience	**Catalog # 553816**; RRID:AB_395068	IHC (1:200)
Antibody	Anti-mouse CD138-PE (rat monoclonal)	BD Bioscience	**Catalog #** 561070; RRID:AB_2033998	FACS (1:500)
Antibody	Anti-mouse cleaved (active) caspase 3-FITC (rabbit monoclonal)	BD Bioscience	**Catalog #** 559341; RRID:AB_397234	FACS (10 µL / sample)
Commercial Assay, Kit	BrdU-APC	BD Bioscience	**Catalog # 552598;** RRID:AB_2861367	Cell proliferation kit
Peptide, recombinant protein	Streptavidin-APC	BD Bioscience	**Catalog #** 554067; RRID:AB_10050396	FACS (1:1000) IF (1:200)
Peptide, recombinant protein	Streptavidin-PE-Cy7	BD Bioscience	**Catalog #** 557598	FACS (1:1000)
Peptide, recombinant protein	Streptavidin-APC-Cy7	BD Bioscience	**Catalog #** 554063; RRID:AB_10050396	FACS (1:1000)
Peptide, recombinant protein	Annexin V-PE	BD Bioscience	**Catalog #** 560930	FACS (1:100)
Chemical compound	7-AAD	BD Bioscience	**Catalog #** 559925; RRID:AB_2869266	FACS (1:1000)
Chemical compound	CellTrace Violet	Invitrogen	**Catalog # C34557**	FACS
Chemical compound	H2DCFDA	Invitrogen	**Catalog # D399**	FACS
Chemical compound	TMRE	Invitrogen	**Catalog # T669**	FACS
Chemical compound	CB839	Cayman	**Catalog #** 22038	Cell culture
Chemical compound	UK5099	Cayman	**Catalog #** 16980	Cell culture
Chemical compound	Hydroxy-chloroquine	Cayman	**Catalog #** 17911	Cell culture
Chemical compound	Menadione	Sigma Aldrich	**Catalog #** 58-27-5	Cell culture
Antibody	Anti-mouse IgM-HRP Ab (Goat polyclonal)	SouthernBiotech	**Catalog #** 1021–05	ELISA (1:1000)
Antibody	Anti-mouse IgG1-HRP Ab (Goat polyclonal)	SouthernBiotech	**Catalog #** 1071–05	ELISA (1:1000)
Antibody	Anti-mouse IgM-Biotin Ab (Goat polyclonal)	SouthernBiotech	**Catalog #** 1021–08	ELISpot (1:1000)
Antibody	Anti-mouse IgG1-Biotin Ab (Goat polyclonal)	SouthernBiotech	**Catalog #** 1070–08	ELISpot (1:1000)
Commercial Assay, Kit	Seahorse XF Glycolysis stress test	Agilent	**Catalog #** 103020–100	Metabolic flux analysis kit
Commercial Assay, Kit	Seahorse XF Mito stress test	Agilent	**Catalog #** 103016–100	Metabolic flux analysis kit
Software	FlowJo	TreeStar → BD Biosciences		Flow cytometry data analysis